Approximate Global Minimizers to Pairwise Interaction Problems via Convex Relaxation*

Mahdi Bandegi[†] and David Shirokoff[‡]

Abstract. We present a new approach for computing approximate global minimizers to a large class of nonlocal pairwise interaction problems defined over probability distributions. The approach predicts candidate global minimizers, with a recovery guarantee, that are sometimes exact, and often within a few percent of the optimum energy (under appropriate normalization of the energy). The procedure relies on a convex relaxation of the pairwise energy that exploits translational symmetry, followed by a recovery procedure that minimizes a relative entropy. Numerical discretizations of the convex relaxation yield a linear programming problem over convex cones that can be solved using well-known methods. One advantage of the approach is that it provides sufficient conditions for global minimizers to a nonconvex quadratic variational problem, in the form of a linear, convex, optimization problem for the autocorrelation of the probability density. We demonstrate the approach in a periodic domain for examples arising from models in materials, social phenomena, and flocking. The approach also exactly recovers the global minimizer when a lattice of Dirac masses solves the convex relaxation. An important by-product of the relaxation is a decomposition of the pairwise energy functional into the sum of a convex functional and nonconvex functional. We observe that in some cases, the nonconvex component of the decomposition can be used to characterize the support of the recovered minimizers.

Key words. global minimizers, nonconvex energy, pairwise interactions, convex relaxations, conic programming, semidefinite programming, flocking, self-assembly

AMS subject classifications. 49M30, 49S05

DOI. 10.1137/16M1069146

1. Introduction. In this paper, we present a new approach for computing candidate global minimizers to a class of energy functionals that arise as continuum approximations to a large collection of interacting particles. Although there are many models for how a collection of particles may interact, we consider here functionals corresponding to systems where particles interact only in pairs with each other. The resulting pairwise energy functionals are in general nonconvex and quadratic, and may have multiple local minimizers, making the global optimization a potentially difficult problem. One could in principle numerically discretize the quadratic functional we consider, using $n \gg 1$ spatial grid points, and arrive at a finite dimensional, quadratic optimization problem. Unfortunately, minimizing such a discrete problem through currently known methods (see [28, sections 4–5] and references within), is computationally prohibitive, and requires $\mathcal{O}(2^n)$ floating point operations. We stress that

^{*}Received by the editors April 5, 2016; accepted for publication (in revised form) by K. Promislow September 14, 2017; published electronically February 6, 2018.

http://www.siam.org/journals/siads/17-1/M106914.html

Funding: This work was supported by a grant from the Simons Foundation (359610, David Shirokoff) and partial support through the National Science Foundation, DMS–1719693 (Shirokoff).

[†]Dept. of Mathematical Sciences, NJIT, Newark, NJ 07102 (mb495@njit.edu).

[‡]Corresponding author. Dept. of Mathematical Sciences, NJIT, Newark, NJ 07102 (david.g.shirokoff@njit.edu).

these computational costs are a currently known upper bound, and future algorithms may improve upon them.

The idea in the new approach is to avoid minimizing the nonconvex quadratic functional, and instead minimize a linear convex functional that bounds the nonconvex functional from below. The solution to this lower bound problem then results in a new sufficient condition for global minimizers. The advantage of this approach is that numerical discretizations of the linear, lower bound problem, using n spatial grid points, require $\mathcal{O}(n)$ linear constraints, and hence may be solved using $\mathcal{O}(n)$ floating point operators. We then obtain candidate minimizers, not by minimizing the original energy, but rather choosing ones that try to satisfy this new sufficient condition. If a candidate satisfies the sufficient condition exactly, then we are guaranteed that it is a global minimum. If a candidate minimizer does not satisfy the condition exactly, then by virtue of the fact that the sufficient condition provides a lower bound to the energy functional, we can quantify a worst case estimate on the energy difference between the candidate and global minimizer.

Although parts of the approach are numerical in nature, a by-product of the analytic formulation is an optimal decomposition of the energy functional into the sum of a non-negative, nonconvex functional, and a convex functional. The resulting convex functional in the decomposition is then highly reminiscent of a convex envelope. This decomposition will also help to explain the emergence of new length scales that characterize the patterns of many interacting particles.

Pair interaction problems are ubiquitous throughout the sciences, appearing in problems ranging from electromagnetics, the weak interaction of nuclear matter [49], biological swarming [5, 18, 40, 43, 59, 60, 61], colloids, polymers [17, 44], consensus [41], mathematical physics [14, 36], and self-assembly [29, 38, 46] to name a few. In these systems, each particle exhibits and experiences a force from every other particle in the system. The resulting sum of the pairwise energies then promotes the collective organization of matter into the formation of structures such as solids or crystalline lattices [16, 54, 55, 56].

Global minimizers or ground states for many particle systems play a key physical role as they often describe the most likely observed state at low temperatures, influence the structure of matter at high temperatures, and are also important for computing phase diagrams [21, 26]. Dynamically, global minimizers appear as steady states to gradient flows or as critical points to Hamiltonian systems, and therefore may play a role in characterizing the long time behavior in some dynamical systems.

We consider problems motivated by a large number, $N \gg 1$, of interacting particles, where a probability measure $\rho(\mathbf{x}) d\mathbf{x}$ is used to represent the distribution of particles. Here $\mathbf{x} \in \mathbb{R}^d$ denotes the spatial coordinates in a dimension $d \geq 1$. For problems on a domain $\Omega \subseteq \mathbb{R}^d$, we consider energy functionals that take the form

(1.1)
$$\mathcal{E}(\rho) := \frac{1}{2} \int_{\Omega} \int_{\Omega} \rho(\mathbf{x}) \rho(\mathbf{y}) W(\mathbf{x} - \mathbf{y}) \, d\mathbf{x} \, d\mathbf{y}.$$

In (1.1), $\rho(\mathbf{x}) d\mathbf{x}$ (resp., $\rho(\mathbf{y}) d\mathbf{y}$) is interpreted as the fraction of particles in the vicinity of a point \mathbf{x} (resp., \mathbf{y}) in the domain Ω . Hence, the energy (1.1) is the double integral over all possible pairs of particles at locations \mathbf{x} and \mathbf{y} , weighted by the *interaction potential* $W(\mathbf{x}-\mathbf{y})$. Physically, $W(\mathbf{r})$ typically represents the energy cost of having two particles separated by the

vector \mathbf{r} . Due to the double integral in (1.1) over all possible pairs of locations \mathbf{x} and \mathbf{y} , we refer to $\mathcal{E}(\rho)$ as the *pairwise energy*.

Formally $\rho(\mathbf{x}) d\mathbf{x}$ will be taken as a probability measure, however, for brevity we will suppress the $d\mathbf{x}$ throughout the written text and write $\rho(\mathbf{x})$ with the understanding that $\rho(\mathbf{x})$ is a measure and includes $L^1(\Omega)$ probability densities and nonclassical functions such as a Dirac mass. Without loss of generality, the total mass m of $\rho(\mathbf{x})$ is taken to be 1:

(1.2)
$$m := \int_{\Omega} \rho(\mathbf{x}) \, d\mathbf{x} = 1.$$

If $\rho(\mathbf{x})$ was normalized to $m \neq 1$ in (1.2), i.e., as the total number of particles in the system m = N, then a rescaling of $\tilde{\rho}(\mathbf{x}) = m^{-1}\rho(\mathbf{x})$ rescales $\mathcal{E}(\rho) = m^2\mathcal{E}(\tilde{\rho})$ by m^2 . As a result, minimizing $\mathcal{E}(\tilde{\rho})$ over $\tilde{\rho}(\mathbf{x})$ with mass 1 is equivalent to minimizing a rescaled $\mathcal{E}(\rho)$ over $\rho(\mathbf{x})$ with mass m. In general, the assumption of (1.2), as opposed to a different value of m, does not alter the approach in this paper.

Remark 1.1. For the purposes of minimizing the energy (1.1) on $\Omega = \mathbb{R}^d$, the interaction potential $W(\mathbf{x})$ may be assumed to be mirror symmetric, i.e., even with respect to the simultaneous negation of the coordinates, for all $\mathbf{x} \in \mathbb{R}^d$, $W(-\mathbf{x}) = W(\mathbf{x})$, where $W(-\mathbf{x}) := W(-x_1, \dots, -x_d)$. If, for instance, $W(\mathbf{x})$ is not mirror symmetric, one may write $W(\mathbf{x}) = W_E(\mathbf{x}) + W_O(\mathbf{x})$, where $W_E(\mathbf{x})$ and $W_O(\mathbf{x})$ are the following even and odd components of $W(\mathbf{x})$:

$$W_E(\mathbf{x}) := \frac{1}{2} \Big(W(\mathbf{x}) + W(-\mathbf{x}) \Big), \quad W_O(\mathbf{x}) := \frac{1}{2} \Big(W(\mathbf{x}) - W(-\mathbf{x}) \Big).$$

The function $W_O(\mathbf{x})$, when inserted into the energy integral (1.1), then integrates to zero by a change of variables:

(1.3)
$$\int_{\mathbb{R}^d} \int_{\mathbb{R}^d} \rho(\mathbf{y}) W_O(\mathbf{x} - \mathbf{y}) \rho(\mathbf{x}) \, d\mathbf{x} \, d\mathbf{y} = \frac{1}{2} \int_{\mathbb{R}^d} \int_{\mathbb{R}^d} \rho(\mathbf{y}) \Big(W(\mathbf{x} - \mathbf{y}) - W(\mathbf{y} - \mathbf{x}) \Big) \rho(\mathbf{x}) \, d\mathbf{x} \, d\mathbf{y} = 0.$$

Hence, the energy $\mathcal{E}(\rho)$ in (1.1) is the same for all $\rho(\mathbf{x})$ regardless of whether $W(\mathbf{x})$ or $W_E(\mathbf{x})$ is used. Therefore, one may assume that $W(\mathbf{x}) = W_E(\mathbf{x})$ is the symmetric component of $W(\mathbf{x})$, even when $W(\mathbf{x})$ is not mirror symmetric. Note that mirror symmetry does not constrain $W(\mathbf{x})$ to be even symmetric in each individual component, i.e., in general one could have $W(x_1, -x_2) \neq W(x_1, x_2)$ and still satisfy $W(-x_1, -x_2) = W(x_1, x_2)$. The same results regarding mirror symmetry hold for the periodic domain $\Omega = [0, 1]^d$.

The approach in this paper will focus on energies of the form (1.1), however, we now briefly discuss how the energy $\mathcal{E}(\rho)$, which is defined for probability measures $\rho(\mathbf{x})$, can be related to the energy of a discrete particle system. For example, restricting $\rho(\mathbf{x})$ in the energy $\mathcal{E}(\rho)$ to a sum of N Dirac masses can be interpreted as the energy of an N particle system. Specifically, substituting an ansatz of Dirac masses into the energy (1.1) yields

(1.4)
$$\mathcal{E}_N(\mathbf{x}_1, \mathbf{x}_2, \dots, \mathbf{x}_N) := \mathcal{E}(\rho_N), \quad \text{where} \quad \rho_N(\mathbf{x}) = \frac{1}{N} \sum_{j=1}^N \delta(\mathbf{x} - \mathbf{x}_j).$$

By direct calculation, and assuming that $W(\mathbf{x})$ is continuous so that the integration against Dirac masses is well defined, one has

(1.5)
$$\mathcal{E}_N(\mathbf{x}_1, \mathbf{x}_2, \dots, \mathbf{x}_N) = \frac{1}{2N^2} \sum_{i=1}^N \sum_{j=1}^N W(\mathbf{x}_i - \mathbf{x}_j).$$

Within the double-sum (1.5) are N terms, where i = j, that result in a total contribution of $(2N)^{-1}W(\mathbf{0})$ to the overall energy \mathcal{E}_N . Provided $W(\mathbf{0}) < \infty$ is bounded¹ at the origin, \mathcal{E}_N can be identified as the energy of N discrete interacting particles—interacting with the same interaction potential $W(\mathbf{x})$ as in (1.1). The calculation also shows that minimizing $\mathcal{E}(\rho)$ over probability measures $\rho(\mathbf{x})$ includes the energies \mathcal{E}_N of all possible arrangements of N particles for any $N \geq 1$.

Remark 1.2 (numerical example: a particle gradient flow for a periodic Morse potential). Arrangements of particles that minimize the collective energy \mathcal{E}_N may form patterns on length scales that are not readily identifiable from the interaction energy $W(\mathbf{x})$. Figure 1 shows the time evolution for a collection of randomly distributed particles undergoing a one dimensional gradient flow governed by the system of ordinary differential equations:

(1.6)
$$\frac{dx_j}{dt} = -\nabla_{x_j} \mathcal{E}_N, \quad 1 \le j \le N.$$

Here the periodic Morse potential (6.3) (with parameters $\sigma = 0.1$, (L, G) = (1.2, 0.9)) was used for \mathcal{E}_N , while the initial particle positions, i.e., x_j at t = 0 for $1 \le j \le N$, was taken to be randomly distributed in the domain [0, 1], sampled from a uniform probability distribution. A total of N = 400 particles was used in the simulation, however, the same histogram shape in Figure 1 was observed in repeated trials, for different values of N = 200 and 600, and also for (slightly perturbed) uniformly distributed initial data. Figure 1 also shows the histogram of particle positions as $t \to \infty$, demonstrating that the particles coalesce into a region with a width of ~ 0.159 units.

Recently, computational methods based on convex relaxations or lower bounds have been used to estimate low energy states and phase diagrams in materials science. For instance, [52] computed convex lower bounds to estimate the order-disorder phase transition in energy functionals containing double-wells. Meanwhile, [32] used relaxations to compute approximate density matrices for quantum systems at zero temperature, while [34, 35, 37] have computed molecular structures.

The approach we present for computing approximate global minimizers is similar in spirit to other state of the art algorithms currently used in optimization theory and integer programming that exploit matrix semidefinite programming (SDP) (see also [6, 23, 42] for a discussion on SDPs and relaxations). For example, semidefinite-based convex relaxations represent some

¹Many interaction potentials are not bounded at $\mathbf{x} = \mathbf{0}$; see, for instance, the divergent power law potentials in [15, 53].

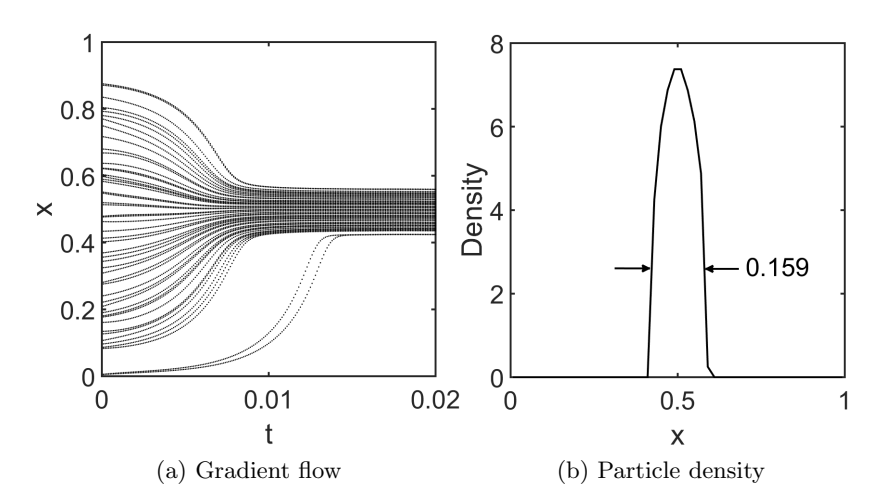


Figure 1. (a) Time evolution of equation (1.6) for the interaction potential (6.3) and N=400 discrete particles (only 50 shown), towards a critical point of \mathcal{E}_N . (b) The density distribution (using 50 bins) of the discrete particles at steady state (i.e., as $t \to \infty$) from part (a). The density is normalized to have area one. The support of the density has an approximate width of ~ 0.159 (computed as the difference between the maximum and minimum particle locations) which is not immediately related to the interaction potential W(x). The width, however, will emerge as the length scale in the optimal dual decomposition for the energy presented in section 5 (see also Figure 5(a)).

of the best known polynomial time algorithms for computing approximate solutions to the graph partitioning problem [25] and matrix completion problem (*Netflix prize*) [11]. They have also been used in data science to approximately solve the k-disjoint clique problem [2] and blind deconvolution [1], while other relaxations have been used to characterize the sparsest element in a discrete set [19].

Our paper is presented as follows: Section 2 introduces the general problem and definition of the recovery guarantee. In section 3 we formulate the convex relaxation, while in section 4 we outline the recovery procedure. Section 5 contains a detailed description of the dual problem and resulting optimal decomposition of the pairwise energy. Sections 7 and 8 present numerical examples in dimensions one and two, respectively. Finally, Appendix A contains information on known cases where the convex relaxation is exact, Appendix B contains numerical details, while Appendix C characterizes solutions to the relaxed problem that take the form of three Dirac masses.

2. Problem formulation and preliminaries. Consider a periodic domain $\Omega = [0, 1]^d$ in dimension d (eventually taken to be d = 1, 2 in sections 6–7), and interaction energy $W(\mathbf{x})$. We are interested in the problem of finding global minimizers to the pairwise energy (1.1):

(P) Minimize
$$\frac{1}{2} \int_{\Omega} \int_{\Omega} \rho(\mathbf{x}) \rho(\mathbf{y}) W(\mathbf{x} - \mathbf{y}) d\mathbf{x} d\mathbf{y}$$

over probability measures $\rho(\mathbf{x}) \in \mathcal{C}_1$ with $\int_{\Omega} \rho(\mathbf{x}) d\mathbf{x} = 1$.

Here we have introduced C_1 as a convex cone to characterize nonnegative measures:²

$$C_1 := \left\{ f \in C^0(\Omega)' : \langle f, u \rangle \ge 0 \text{ for all } u \in C^0(\Omega) \text{ with } u(\mathbf{x}) \ge 0 \right\},$$

where

$$\langle f, u \rangle = \int_{\Omega} u(\mathbf{x}) f(\mathbf{x}) \, d\mathbf{x}$$

is the integral of the continuous function $u(\mathbf{x})$ against the measure $f(\mathbf{x}) d\mathbf{x}$. In the case when $\rho(\mathbf{x})$ is a classical function, we may equivalently replace C_1 with $\rho(\mathbf{x}) \geq 0$ for all $\mathbf{x} \in \Omega$. In the problem (P), we further assume that $W(\mathbf{x})$ satisfies the following properties:

- (W1) Mirror symmetric: $W(\mathbf{x}) = W(-\mathbf{x})$, holds for all \mathbf{x} (see Remark 1.1 for justification).
- (W2) Continuous on Ω .
- (W3) Periodic with period 1: $W(\mathbf{x} + \mathbf{k}) = W(\mathbf{x})$ for all $\mathbf{x} \in \Omega$ and integer vectors $\mathbf{k} \in \mathbb{Z}^d$.
- (W4) Normalized with mean zero: $\int_{\Omega} W(\mathbf{x}) d\mathbf{x} = 0$. In such a case, the minimum to (P) is at most zero since $\mathcal{E}(1) = 0$. Note that one can always add, without loss of generality, a constant to $W(\mathbf{x})$.

Remark 2.1. For numerical simplicity we have intentionally limited the problem (P) to continuous interaction potentials $W(\mathbf{x})$ on periodic domains Ω . Many of the results presented here apply to other domains as well, including the sphere or \mathbb{R}^d . For instance, when $\Omega = \mathbb{R}^d$, one may still define a convex relaxation for problem (P). In this case, the countable wavenumbers (i.e., Fourier series) used to define the relaxation in section 3 for the periodic domain $[0,1]^d$ will be replaced with a continuous set of wavenumbers (i.e., Fourier transform). Additional difficulties, not encountered here, may arise in the numerical solution when the domain is unbounded.

For the problems we consider where Ω is compact, (P) admits a global minimum $\mathcal{E}_0 := \mathcal{E}(\rho_0)$, achieved by some probability measure $\rho_0(\mathbf{x})$. Note that $\rho_0(\mathbf{x})$ is not unique since $\mathcal{E}(\rho)$ is invariant under translations so that $\rho_0(\mathbf{x} + \mathbf{s})$ is also a global minimum for any \mathbf{s} . For noncompact domains, the existence and uniqueness [13, 15, 53] (up to translations and rotations) of global minimizers is more subtle since mass can be spread arbitrarily far apart (see also [3, 4, 8] for results on the structure of minimizers).

We now review several necessary conditions imposed by the first and second variation of $\mathcal{E}(\rho)$ that a global minimizer $\rho_0(\mathbf{x})$ must satisfy (see [5] for a discussion and [12] for a rigorous treatment). First, a candidate global minimizer $\rho^*(\mathbf{x})$ satisfies the first order necessary conditions if the first variation of $\mathcal{E}(\rho)$,

(2.1)
$$\Lambda(\mathbf{x}) := \int_{\Omega} W(\mathbf{x} - \mathbf{y}) \rho^*(\mathbf{y}) \, d\mathbf{y},$$

²In the definition of C_1 , $C^0(\Omega)$ is the space of periodic continuous functions on Ω endowed with the sup norm. Since $\Omega = [0,1]^d$ is compact, the functions $u \in C^0(\Omega)$ are bounded and also form a Banach space. The notation here, $\langle f, u \rangle$, represents the pairing of elements f in the dual space $C^0(\Omega)'$ with continuous functions u that are elements of $C^0(\Omega)$ (see [24, Chapter 5] for a general discussion on Banach spaces). In addition, the Riesz representation theorem for bounded continuous functions (see [24, Chapter 7], or [48, Chapter 2]) shows that elements in $C^0(\Omega)'$ can be identified as nonnegative *Borel measures*, which justifies the integral representation of $\langle f, u \rangle$.

satisfies

(2.2)
$$\Lambda(\mathbf{x}) = 2\mu \quad \text{for all } \mathbf{x} \in S_* := \text{supp}(\rho^*),$$

(2.3)
$$\Lambda(\mathbf{x}) \geq 2\mu \quad \text{for all } \mathbf{x} \in \Omega \text{ (including } \mathbf{x} \notin S_*).$$

Here supp(f) is the support of $f(\mathbf{x})$, i.e., the set where $f(\mathbf{x})$ does not vanish,³ while $\mu \in \mathbb{R}$ is a Lagrange multiplier constant. Note that multiplying (2.2) by $\rho^*(\mathbf{x})$ and integrating over Ω shows that $\mathcal{E}(\rho^*) = \mu$. Hence, if $\rho^*(\mathbf{x})$ satisfies the first order condition (2.2), then $\rho^*(\mathbf{x})$ has energy μ . As a result, setting $\mu = \mathcal{E}_0$ in (2.2) shows that the global minimizer $\rho_0(\mathbf{x})$ satisfies

(2.4)
$$\int_{\Omega} W(\mathbf{x} - \mathbf{y}) \rho_0(\mathbf{y}) \, d\mathbf{y} = 2\mathcal{E}_0 \quad \text{for all } \mathbf{x} \in S_0 := \text{supp}(\rho_0).$$

One difficulty with using condition (2.4) to solve for $\rho_0(\mathbf{x})$ is that both \mathcal{E}_0 and S_0 are not known a priori. As implied by the integral equation in [5] (see [12, Remark 2.5] for a rigorous treatment), consideration of the second variation of $\mathcal{E}(\rho)$ will show that knowledge of S_0 alone will be sufficient to compute $\rho_0(\mathbf{x})$ through a convex optimization problem. Specifically, a candidate $\rho^*(\mathbf{x})$ satisfies the second order necessary conditions for a global minimum if the second variation is nonnegative (within the class of perturbations that make the first variation vanish):

(2.5)
$$\mathcal{E}(f) \geq 0$$
 for finite measures $f(\mathbf{x})$ with $\int_{\Omega} f(\mathbf{x}) d\mathbf{x} = 0$ and $\operatorname{supp}(f) \subseteq S_*$.

Here the class of $f(\mathbf{x})$'s in (2.5) are exactly the measures that when integrated against $\Lambda(\mathbf{x})$ vanish. Equation (2.5) also implies the following remark regarding the convexity of $\mathcal{E}(\rho)$ when restricted to probabilities having supports in S_* .

Remark 2.2 (the importance of S_0). Examining the necessary condition in (2.5) when $\rho_0(\mathbf{x})$ is a global minimum, one has the following observations:

(i) Condition (2.5) implies that

$$\mathcal{E}(\rho)$$
 is convex when restricted to $\mathcal{B} := \left\{ \rho(\mathbf{x}) \in \mathcal{C}_1, \int_{\Omega} \rho(\mathbf{x}) \, \mathrm{d}\mathbf{x} = 1, \ \mathrm{supp}(\rho) \subseteq S_0 \right\}.$

(ii) Knowledge of the support of $\rho_0(\mathbf{x})$, i.e., the set S_0 , implies that (P) may be formulated as a convex optimization problem.

Note that \mathcal{B} is a convex set. To show (i), take any $\rho_1(\mathbf{x}), \rho_2(\mathbf{x}) \in \mathcal{B}$ and set $f(\mathbf{x}) := \rho_1(\mathbf{x}) - \rho_2(\mathbf{x})$. Therefore, $f(\mathbf{x})$ has support in S_0 and satisfies the criteria in (2.5). Then, by direct calculation using the fact that $\mathcal{E}(\rho)$ is quadratic, one has for any $0 \le \lambda \le 1$,

(2.6)
$$0 \leq (1 - \lambda)\lambda \,\mathcal{E}(f) = \lambda \mathcal{E}(\rho_1) + (1 - \lambda)\mathcal{E}(\rho_2) - \mathcal{E}(\lambda \rho_1 + (1 - \lambda)\rho_2)$$
$$\Rightarrow \mathcal{E}(\lambda \rho_1 + (1 - \lambda)\rho_2) \leq \lambda \mathcal{E}(\rho_1) + (1 - \lambda)\mathcal{E}(\rho_2).$$

³If $f(\mathbf{x})$ is a continuous function on Ω , then $\operatorname{supp}(f) = \operatorname{cl}\{\mathbf{x} : f(\mathbf{x}) \neq 0\}$, where cl denotes the closure. See [24, Chapter 7] for the definition when $f(\mathbf{x})$ is a measure.

The inequality (2.6) shows that $\mathcal{E}(\rho)$ is convex when restricted to probabilities in \mathcal{B} . For (ii), note that $\rho_0(\mathbf{x}) \in \mathcal{B}$, so that restricting the optimization of $\mathcal{E}(\rho)$ in (P) to the space \mathcal{B} produces the same minimum \mathcal{E}_0 . Moreover, (P) then becomes the following convex problem,

$$\min \mathcal{E}(\rho)$$
, subject to $\rho(\mathbf{x}) \in \mathcal{B}$.

Remark 2.2 highlights the importance of finding sets S_* , where $\mathcal{E}(\rho)$ is convex. In our approach, we do not have a proof that the recovered candidate minimizers satisfy the first and second order necessary conditions; however, in section 5 we provide new sufficient conditions for $\mathcal{E}(\rho)$ to be convex when $\sup(\rho) \subseteq S_*$. Sections 6–7 then demonstrate that our recovered minimizers often satisfy this new sufficient condition.

A common practice in optimization theory is to guarantee that a candidate minimizer (or maximizer) is within a factor α of the optimal value. Here we say that an approximate minimizer $\rho^*(\mathbf{x})$ to problem (P) has an (α, ν) guarantee, where $0 \le \alpha \le 1$, $\nu \ge \mathcal{E}_0$, if the shifted energy $\mathcal{E}(\rho^*) - \nu$ is optimal to within a factor of α :

$$(\mathcal{E}_0 - \nu) \le \mathcal{E}(\rho^*) - \nu \le \alpha(\mathcal{E}_0 - \nu).$$

In the context of gradient flows on $\mathcal{E}(\rho)$, one may always add an arbitrary constant to the underlying potential $W(\mathbf{x})$ and, hence, $\mathcal{E}(\rho)$, without affecting the dynamics of $\rho(\mathbf{x})$. To eliminate the ambiguity of adding such an arbitrary constant, we introduce the shift $\nu = \mathcal{E}(\rho_{ref})$ as a reference energy with respect to a base probability $\rho_{ref}(\mathbf{x})$.

Clearly, if $\alpha = 1$ with any ν then $\mathcal{E}(\rho^*) = \mathcal{E}_0$ and, hence, $\rho^*(\mathbf{x})$ is a global minimizer. In this case, we drop the notation ν and simply say the solution $\rho^*(\mathbf{x})$ is optimal with a guarantee $\alpha = 1$. In the numerical section of this paper we always report an α guarantee with $\nu = 0$. Due to the normalization (W4), $\nu = \mathcal{E}(1) = 0$ corresponds to the constant state $\rho_{ref}(\mathbf{x}) = 1$.

In general, problem (P) is difficult to solve since the energy $\mathcal{E}(\rho)$ is a nonconvex functional of $\rho(\mathbf{x})$. In the next section we will show how to replace (P) with a convex relaxation (R) that is more amenable to analysis. We will

- 1. formulate a convex relaxation (R) of (P);
- 2. solve the relaxation (R) using efficient linear programming algorithms;
- 3. recover a candidate minimizer from (R) using minimal points of the Kullback-Leibler divergence, and report an (α, ν) guarantee for the candidate minimizer (with $\nu = 0$).
- **3.** The convex relaxation. The purpose of this section is to formulate a convex relaxation of (P) that takes the form of a constrained linear optimization problem. The linear optimization problem may then be numerically approximated and solved using linear programming techniques.

To obtain the relaxation, we first rewrite $\mathcal{E}(\rho)$ by performing a coordinate change of variables in the integral. Letting $\mathbf{s} = \mathbf{x} - \mathbf{y}$,

$$\mathcal{E}(\rho) = \frac{1}{2} \int_{\Omega} \int_{\Omega} \rho(\mathbf{x}) \rho(\mathbf{x} + \mathbf{s}) W(\mathbf{s}) \, d\mathbf{x} \, d\mathbf{s} = \frac{1}{2} \langle F, W \rangle,$$
$$F(\mathbf{s}) := \int_{\Omega} \rho(\mathbf{x}) \rho(\mathbf{x} + \mathbf{s}) \, d\mathbf{x} = \rho \circ \rho.$$

Here we have introduced $F(\mathbf{x})$ as the auto-correlation of $\rho(\mathbf{x})$, along with a shorthand binary operator notation \circ . In addition, we assume that $\rho(\mathbf{x})$ is defined periodically on Ω so that $F(\mathbf{x})$ is also periodic on Ω .

The original problem (P) can then be understood as minimizing a linear functional $\langle F, W \rangle$, over the space of elements $F(\mathbf{x}) \in \mathcal{A}$ that arise as the auto-correlations of probabilities:

$$\mathcal{A} := \left\{ F : F(\mathbf{s}) = \int_{\Omega} \rho(\mathbf{x}) \rho(\mathbf{x} + \mathbf{s}) \, \mathrm{d}\mathbf{x}, \text{ such that } \rho \in \mathcal{C}_1, \int_{\Omega} \rho(\mathbf{x}) \, \mathrm{d}\mathbf{x} = 1 \right\}.$$

We will show below that \mathcal{A} is not a convex space (see Remark 3.2). Hence, we have reformulated the original problem (P) of minimizing a nonconvex objective functional over a convex set, to the minimization of a linear, convex functional over a nonconvex set. Our goal is now to relax the admissible space of functions \mathcal{A} to a convex set. Ideally, one would like to use the smallest convex relaxation, i.e., the convex hull of \mathcal{A} ; however, we use a space of convex cones that may be exploited in subsequent numerical computations. Specifically, since $F(\mathbf{x})$ is defined in the periodic domain Ω , it is natural to consider representations as a Fourier series. The following proposition, which characterizes several well-known properties of auto-correlations, will play an important role in defining the relaxation.

Proposition 3.1 (properties of A). Given any $F(\mathbf{x}) \in A$, the following properties hold:

- (A1) $F(\mathbf{x})$ is nonnegative, i.e., for any nonnegative continuous function $u(\mathbf{x}) \geq 0$, $\langle F, u \rangle \geq 0$.
- (A2) $F(\mathbf{x})$ integrates to one: $\langle F, 1 \rangle = 1$.
- (A3) $F(\mathbf{x})$ is mirror symmetric about the origin, i.e., $F(-\mathbf{x}) = F(\mathbf{x})$, corresponding to zero sine modes. For every $\mathbf{k} \in \mathbb{Z}^d$, $\mathbf{k} \neq \mathbf{0}$, $\langle F, \sin(2\pi \mathbf{k} \cdot \mathbf{x}) \rangle = 0$.
- (A4) $F(\mathbf{x})$ has nonnegative cosine modes. For every $\mathbf{k} \in \mathbb{Z}^d$, $\mathbf{k} \neq \mathbf{0}$, $\langle F, \cos(2\pi \mathbf{k} \cdot \mathbf{x}) \rangle \geq 0$. Here \mathbb{Z}^d is the set of integers defined by

$$\mathbb{Z}^d = \{(n_1, \dots, n_d) : \text{ for integers } n_j, \ 0 \le j \le d\}.$$

Note that values of $-\mathbf{k}$ in properties (A3)–(A4) characterize the same constraints as \mathbf{k} , and are therefore redundant. We will, however retain all $\mathbf{k} \in \mathbb{Z}^d$ to simplify subsequent notation.

Proof. The proof of (A1)–(A4) is straightforward and done by a direct calculation of the appropriate integrals $\langle \cdot, \cdot \rangle$. If $F(\mathbf{x}) \in \mathcal{A}$, then $F(\mathbf{s}) = \int_{\Omega} \rho(\mathbf{x}) \rho(\mathbf{x} + \mathbf{s}) d\mathbf{x}$ for some $\rho(\mathbf{x}) \in \mathcal{C}_1$. The integral $\langle F, u \rangle$ can then be written as:

$$\langle F, u \rangle = \int_{\Omega} \int_{\Omega} \rho(\mathbf{x}) \rho(\mathbf{y}) u(\mathbf{x} - \mathbf{y}) \, d\mathbf{x} \, d\mathbf{y} = \langle \rho, U \rangle, \text{ where } U(\mathbf{x}) := \int_{\Omega} \rho(\mathbf{y}) u(\mathbf{x} - \mathbf{y}) \, d\mathbf{y}.$$

For (A1), take any continuous, nonnegative function $u(\mathbf{x}) \geq 0$ to integrate against $F(\mathbf{x})$. Then, since $\rho(\mathbf{x}) \in \mathcal{C}_1$, the function $U(\mathbf{x}) \geq 0$ is nonnegative, and also continuous since it is a convolution. Hence, integrating $U(\mathbf{x})$ against $\rho(\mathbf{x})$ is also nonnegative, implying $\langle F, u \rangle = \langle \rho, U \rangle \geq 0$.

For (A2), taking $u(\mathbf{x}) = 1$ in the definition for $U(\mathbf{x})$ implies that $U(\mathbf{x}) = 1$. It then follows that $\langle F, 1 \rangle = \langle \rho, 1 \rangle = 1$.

For (A3), integrating $F(\mathbf{x})$ against any sine mode, $\sin(2\pi\mathbf{k}\cdot\mathbf{x})$, yields

$$\langle F, \sin(2\pi \mathbf{k} \cdot \mathbf{x}) \rangle = \int_{\Omega} \int_{\Omega} \rho(\mathbf{x}) \rho(\mathbf{y}) \Big(\sin(2\pi \mathbf{k} \cdot \mathbf{x}) \cos(2\pi \mathbf{k} \cdot \mathbf{y}) - \sin(2\pi \mathbf{k} \cdot \mathbf{y}) \cos(2\pi \mathbf{k} \cdot \mathbf{x}) \Big) d\mathbf{x} d\mathbf{y}$$
$$= 0.$$

Note also that a similar calculation shows that $F(\mathbf{x})$ is mirror symmetric, i.e., for any continuous function $u(\mathbf{x})$, one has $\langle F(-\mathbf{x}), u(\mathbf{x}) \rangle = \langle F(\mathbf{x}), u(\mathbf{x}) \rangle$. Here, $(-\mathbf{x})$ denotes the simultaneous negation of all coordinates (see also Remark 1.1).

Finally, for (A4), integrating $F(\mathbf{x})$ against any cosine mode, $\cos(2\pi\mathbf{k}\cdot\mathbf{x})$, yields

$$\langle F, \cos(2\pi \mathbf{k} \cdot \mathbf{x}) \rangle = \int_{\Omega} \int_{\Omega} \rho(\mathbf{x}) \rho(\mathbf{y}) \cos(2\pi \mathbf{k} \cdot (\mathbf{x} - \mathbf{y})) \, d\mathbf{x} \, d\mathbf{y}$$
$$= |\langle \rho, \cos(2\pi \mathbf{k} \cdot \mathbf{x}) \rangle|^2 + |\langle \rho, \sin(2\pi \mathbf{k} \cdot \mathbf{x}) \rangle|^2 \ge 0.$$

Remark 3.2 (the set \mathcal{A} is not convex). To show that \mathcal{A} is not convex take $f_1(x) = 1 + \cos(2\pi x)$ and $f_2(x) = 1 + \cos(2n\pi x)$ on $\Omega = [0, 1]$, where $n \gg 1$ is a large integer. The convex combination of

$$\lambda(f_1 \circ f_1) + (1 - \lambda)(f_2 \circ f_2) = 1 + \frac{1}{4}\cos(2\pi x) + \frac{1}{4}\cos(2n\pi x),$$

when $\lambda = \frac{1}{2}$, must come from an auto-correlation of a function taking the form (with arbitrary phases φ_1, φ_2)

$$f_3(x) = 1 + \frac{1}{\sqrt{2}}\cos(2\pi x - \varphi_1) + \frac{1}{\sqrt{2}}\cos(2n\pi x - \varphi_2).$$

Choosing n large enough, the minimum value of $f_3(x)$, regardless of the values φ_1 , φ_2 , can be made arbitrarily close to $1 - \sqrt{2} < 0$. Hence, for sufficiently large n, there is no nonnegative function $f_3(x)$ with auto-correlation $(\lambda f_1 \circ f_1 + (1 - \lambda)f_2 \circ f_2)$.

Properties (A1)–(A2) characterize $F(\mathbf{x}) \in \mathcal{A}$ as a probability measure, and therefore show that the set \mathcal{A} is a subset of the convex cone \mathcal{C}_1 , i.e., $\mathcal{A} \subseteq \mathcal{C}_1$. Properties (A3)–(A4) are related to a standard result in signal processing—that the Fourier series of an auto-correlation is a power spectrum. In the case at hand, (A3)–(A4) motivate the definition of a second convex cone, \mathcal{C}_2 , defined by measures having nonnegative cosine modes and zero sine modes:

(3.1)
$$\mathcal{C}_2 := \left\{ f \in C^0(\Omega)' : \langle f, \cos(2\pi \mathbf{k} \cdot \mathbf{x}) \rangle \ge 0, \ \langle f, \sin(2\pi \mathbf{k} \cdot \mathbf{x}) \rangle = 0, \ \forall \ \mathbf{k} \in \mathbb{Z}^d \setminus \mathbf{0} \right\}.$$

Hence, properties (A3)–(A4) show that the set \mathcal{A} is also a subset of \mathcal{C}_2 , i.e., $\mathcal{A} \subseteq \mathcal{C}_2$. Finally, taking the properties (A1)–(A4) together, we define the set

$$\mathcal{C} := \left\{ f \in C^0(\Omega)' : \text{ for all continuous } u(\mathbf{x}) \ge 0, \text{ and } \mathbf{k} \in \mathbb{Z}^d \setminus \mathbf{0}, \\ \left\langle f, \cos(2\pi \mathbf{k} \cdot \mathbf{x}) \right\rangle \ge 0, \quad \left\langle f, u(\mathbf{x}) \right\rangle \ge 0, \\ \left\langle f, \sin(2\pi \mathbf{k} \cdot \mathbf{x}) \right\rangle = 0, \quad \left\langle f, 1 \right\rangle = 1 \right\}.$$

Proposition 3.1 may then be alternatively stated as \mathcal{A} is a subset of \mathcal{C} , i.e., $\mathcal{A} \subseteq \mathcal{C}$. Our goal now is to extend the nonconvex set \mathcal{A} , in the optimization of (P), to a relaxed set \mathcal{C} . The purpose of introducing \mathcal{C}_1 and \mathcal{C}_2 is to identify the set \mathcal{C} as a convex subset of a convex cone. To this end, we make the following remarks characterizing \mathcal{C} .

Remark 3.3 (the set \mathcal{C} is a convex cone with an affine constraint). The set \mathcal{C} is defined through linear constraints and inequalities and, hence, is a convex set. However, \mathcal{C} may also be written alternatively as

$$C = \Big\{ f : f \in C_1 \cap C_2, \text{ and } \langle f, 1 \rangle = 1 \Big\}.$$

Here we have used the cones C_1 and C_2 to represent the properties (A1), (A3), and (A4) in the definition of C. Since both C_1 and C_2 are convex cones, by the intersection properties of convex cones, it follows that $C_1 \cap C_2$ is also a convex cone. As a result, the set C may be interpreted as the convex cone $C_1 \cap C_2$, whose elements satisfy the additional affine constraint $\langle f, 1 \rangle = 1$.

Remark 3.4 (the set \mathcal{C} contains elements that are not in \mathcal{A}). Consider $\Omega = [0,1]$ and $F(x) = 1 + \cos(2\pi x) \in \mathcal{C}$. Then, only functions of the form $f(x) = 1 + \sqrt{2}\cos(2\pi x - \varphi)$ for any φ , have auto-correlations equal to F(x). Since f(x) contains negative values, then $f(x) \notin \mathcal{C}_1$ showing that $F(x) \notin \mathcal{A}$. Moreover, a similar calculation shows that F(x) cannot be written as the convex combination of two, or even a finite number of, elements in \mathcal{A} , i.e., $F(x) \neq \lambda f_1 \circ f_1 + (1 - \lambda) f_2 \circ f_2$ for probabilities $f_1(x)$ and $f_2(x)$ and $f_3(x)$ and $f_3(x)$ cannot be approximated by convex combinations of elements in \mathcal{A} .

We now define the relaxed problem by extending the set A to the convex set C:

(R) Minimize
$$\frac{1}{2}\langle F, W \rangle$$

subject to $\langle F, \cos(2\pi \mathbf{k} \cdot \mathbf{x}) \rangle \ge 0$, $\langle F, u(\mathbf{x}) \rangle \ge 0$, $\langle F, \sin(2\pi \mathbf{k} \cdot \mathbf{x}) \rangle = 0$, $\langle F, 1 \rangle = 1$

for all integers $\mathbf{k} \in \mathbb{Z}^d \setminus \mathbf{0}$ and nonnegative continuous functions $u(\mathbf{x}) \geq 0$.

We denote any solution to (R) as $F_R(\mathbf{x})$ and set $\mathcal{E}_R = \frac{1}{2} \langle F_R, W \rangle$. Moreover, we note that \mathcal{E}_R is a lower bound to \mathcal{E}_0 , i.e., $\mathcal{E}_0 \geq \mathcal{E}_R$, since (R) can be understood as optimizing (P) over a feasible set \mathcal{C} that contains \mathcal{A} .

As discussed in Remark 3.3, the constraints in (R) are both (i) linear in $F(\mathbf{x})$ and (ii) (up to the affine constraint $\langle F, 1 \rangle = 1$) restricted to lie in the convex cone $\mathcal{C}_1 \cap \mathcal{C}_2$. This will lead to numerical discretizations of (R) that take the form of a *conic linear programming* problem. Note that in practice when solving (R), it is often better to enforce the mirror symmetry of $F(\mathbf{x})$ directly, and remove redundant \mathbf{k} values (i.e., \mathbf{k} and $-\mathbf{k}$ yield the same constraint) for the cosine constraints. This will also allow for the removal of the sine constraints in (R), and reduce the size of the domain Ω , and hence the optimization problem. A few remarks are now in order.

Remark 3.5 (sufficient conditions for a global minimizer). The relaxation (R) may in some cases verify that a candidate minimizer $\rho^*(\mathbf{x})$ solves (P). Suppose $\rho^*(\mathbf{x})$ is a probability distribution with auto-correlation $F_R(\mathbf{x})$. Then, since any probability distribution is by definition

larger than the minimizer $\mathcal{E}(\rho^*) = \mathcal{E}_R \geq \mathcal{E}_0 \geq \mathcal{E}_R$. Therefore, one has $\mathcal{E}_R = \mathcal{E}_0$, which implies that $\rho_0(\mathbf{x}) = \rho^*(\mathbf{x})$ is a, possibly nonunique, global minimum.

Remark 3.6 (lattices are exact). If the solution $F_R(\mathbf{x})$ forms a periodic lattice pattern⁴ $\chi \subset \Omega$,

(3.2)
$$F_R(\mathbf{x}) = \frac{1}{|\chi|} \sum_{\mathbf{s} \in \chi} \delta(\mathbf{x} - \mathbf{s}),$$

where $|\chi|$ is the number of points in the lattice pattern, then the relaxation is exact. For solutions of the form (3.2), $F_R \circ F_R = F_R(\mathbf{x})$. Hence, taking $\rho^*(\mathbf{x}) = F_R(\mathbf{x})$ satisfies $F_R(\mathbf{x}) = \rho^* \circ \rho^*$ thereby implying that a lattice is the global minimizer.

Minimizers that take the form of a lattice are of great physical interest, as they explain why matter may form crystal structures. Proofs that particle models, in the large particle number limit, exhibit lattice minimizers have been done for sticky disk models [27, 45], Lennard–Jones-type interaction potentials [57], and energies which include the sum of Lennard–Jones interaction potentials and three particle interactions [20, 22].

In Appendix B, we discuss how to numerically discretize and solve (R). In general, we observe that numerical solutions converge to either (i) classical functions $F_R(\mathbf{x})$ that are continuous, i.e., $F_R(\mathbf{x}) \in \mathcal{C}^0(\Omega)$, or (ii) nonclassical functions $F_R(\mathbf{x})$ that consist of a finite collection of Dirac point masses. Motivated by Remark 3.5, the following section presents one approach for recovering a candidate minimizer $\rho^*(\mathbf{x})$ using $F_R(\mathbf{x})$.

In the case when $F_R(\mathbf{x})$ is a collection of Dirac masses, we will expect recovered candidates $\rho^*(\mathbf{x})$ to also be a collection of Dirac masses. This is because the auto-correlation of a discrete set of Dirac masses is a discrete set of Dirac masses. In contrast, when $F_R(\mathbf{x})$ is a continuous function, we will expect $\rho^*(\mathbf{x})$ to be in $L^2(\Omega)$, and typically take the form of a piece-wise continuous function, i.e., since the auto-correlation of a piece-wise continuous function is continuous.

4. Recovering $\rho^*(x)$ from $F_R(x)$ by minimizing a relative entropy. In this section we outline a procedure for recovering a candidate global minimizer $\rho^*(\mathbf{x})$ from knowledge of the solution to (R), i.e., $F_R(\mathbf{x})$. In general, the relaxed space \mathcal{C} , and therefore solutions to problem (R) may include measures that are not auto-correlations of probabilities (see Remark 3.4). Hence, $\mathcal{A} \subset \mathcal{C}$ is only a proper subset of \mathcal{C} and, as a result, the solution $F_R(\mathbf{x})$ may not come from an auto-correlation of a probability distribution.

The problem of recovering $\rho^*(\mathbf{x})$ from $F_R(\mathbf{x})$ is equivalent to deauto-correlating a function $F(\mathbf{x}) \in \mathcal{C}$, with the caveat that the source function $\rho^*(\mathbf{x})$ is also a probability distribution. The additional nonnegativity restriction, i.e., $\rho^*(\mathbf{x}) \in \mathcal{C}_1$, distinguishes the phase recovery problem at hand from other phase recovery problems recently studied in the context of signal

⁴ A lattice X is the infinite array of discrete points defined by a set of primitive vectors $\mathbf{v}_j \colon X = \{\sum_{j=1}^d n_j \mathbf{v}_j \colon n_j \in \mathbb{Z}, \text{ for } 1 \leq j \leq d\}$. Take $\chi = X \cap \Omega$ as the points in X restricted to the computational domain. Hence χ may be defined for any X. We refer here to χ as a lattice pattern if X can be written as translated copies of χ : $X = \bigcup_{\vec{n} \in \mathbb{Z}^d} (\chi + \vec{n})$. Note that χ may be a set that is larger than one containing the primitive lattice vectors, and that X cannot always be written as the collection of translated copies of χ (in which case χ would not be a lattice pattern).

processing [9, 10, 11, 30, 58]. In our recovery process we follow a procedure introduced by Schulz and Snyder [50] (see also [51]) which chooses $\rho^*(\mathbf{x})$ as a minimizer of the Kullback–Leibler divergence functional (also known as the information divergence) between $F_R(\mathbf{x})$ and the auto-correlation $F_{\rho}(\mathbf{x}) = \rho \circ \rho$. As discussed in [50] (and references within) the information divergence functional has many nice properties for the recovery of nonnegative signals making it a natural choice for the recovery of $\rho^*(\mathbf{x})$.

In this discussion we assume that $F_R(\mathbf{x}) \in \mathcal{C} \cap C^0(\Omega)$ is a continuous function; however, the approach here can also be extended to handle cases where $F_R(\mathbf{x})$ is a collection of discrete Delta masses. The Kullback–Leibler divergence is defined as

(4.1)
$$\mathcal{F}(\rho) := \int_{\Omega} F_R(\mathbf{x}) \ln \left(\frac{F_R(\mathbf{x})}{F_{\rho}(\mathbf{x})} \right) d\mathbf{x} = \int_{\Omega} F_R(\mathbf{x}) \ln \left(\frac{F_R(\mathbf{x})}{\rho \circ \rho} \right) d\mathbf{x},$$

where we assume that $\rho(\mathbf{x}) \in \mathcal{C} \cap L^2(\Omega)$ with $\int_{\Omega} \rho(\mathbf{x}) d\mathbf{x} = 1$. In the definition of $\mathcal{F}(\rho)$, one adopts the conventions

(4.2)
$$0 \ln \frac{0}{a} := 0, \qquad 0 \ln \frac{0}{0} := 0, \qquad a \ln \frac{a}{0} := \infty,$$

to allow for both $F_R(\mathbf{x})$ and $\rho \circ \rho$ to vanish on some set.

Viewing both $F_R(\mathbf{x})$ and $F_{\rho}(\mathbf{x})$ as probability distributions, the Kullback-Leibler divergence, defined by $\mathcal{F}(\rho)$, measures the mismatch between probabilities $F_R(\mathbf{x})$ and $F_{\rho}(\mathbf{x})$. Although $\mathcal{F}(\rho)$ does not define a metric between $F_R(\mathbf{x})$ and $F_{\rho}(\mathbf{x})$, for instance, since it is not symmetric, it is always nonnegative $\mathcal{F}(\rho) \geq 0$, and may still be used to guarantee an exact match between $F_R(\mathbf{x})$ and $F_{\rho}(\mathbf{x})$. Specifically, $\mathcal{F}(\rho^*) = 0$ only when $F_R(\mathbf{x}) = F_{\rho}(\mathbf{x})$ (see, for instance, Pinsker's inequality in [39, Chapter 2]). Hence, in light of Remark 3.5, we have the following alternative sufficient condition for a global minimizer—which motivates the minimization of $\mathcal{F}(\rho)$.

Remark 4.1 (equivalent sufficient condition for a global minimizer). Let $F_R(\mathbf{x})$ solve (R). Then if $\mathcal{F}(\rho^*) = 0$, it follows that $\rho^*(\mathbf{x})$ solves (P). For instance, if $\mathcal{F}(\rho^*) = 0$, then the two auto-correlations are equal: $F_R(\mathbf{x}) = F_{\rho^*}(\mathbf{x}) = \rho^* \circ \rho^*$, so that the conditions in Remark 3.5 are satisfied.

To compute minimizers of $\mathcal{F}(\rho)$ we use the Schulz–Snyder iterative algorithm,⁵ which is an iterative method on the space of nonnegative probabilities. The advantage of the Schulz–Snyder algorithm is not only that it minimizes the functional $\mathcal{F}(\rho)$, but the iterations naturally enforce the probability constraints. As a result, the algorithm is very easy to implement.

We now briefly summarize the derivation, and properties of the Schulz-Snyder algorithm. The idea is to iterate the Euler-Lagrange equation that one obtains by taking the first variation of $\mathcal{F}(\rho)$. Namely, the Euler-Lagrange equation of (4.1) is given as follows: For any mean zero perturbation $g(\mathbf{x})$ whose support is contained in the support of $\rho^*(\mathbf{x})$, the first variation

⁵In the original paper [50], the functional $\mathcal{F}(\rho) + \int_{\Omega} F_R(\mathbf{x}) - F_{\rho}(\mathbf{x}) d\mathbf{x}$ was used instead of $\mathcal{F}(\rho)$. Due to the fact that the Schulz-Snyder iterative algorithm conserves the constraint $\int_{\Omega} F_{\rho}(\mathbf{x}) d\mathbf{x} = 1$, the discrepancy in the functional definition has no effect on the algorithm or results.

vanishes.

(4.3)
$$\int_{\Omega} g(\mathbf{x}) \frac{\delta \mathcal{F}}{\delta \rho}(\rho^*) = 0 \implies \frac{\delta \mathcal{F}}{\delta \rho}(\rho^*) = \text{const. for any } \mathbf{x} \in \text{supp}(\rho^*).$$

By direct calculation, the (unconstrained) L^2 variation of $\mathcal{F}(\rho)$ is

(4.4)
$$\frac{\delta \mathcal{F}}{\delta \rho}(\rho) = -2 \int_{\Omega} \rho(\mathbf{x} + \mathbf{y}) \frac{F_R(\mathbf{y})}{F_\rho(\mathbf{y})} \, d\mathbf{y}.$$

Hence, multiplying (4.4) by $\rho^*(\mathbf{x})$ and integrating over space yields the constant in (4.3). Critical points of $\mathcal{F}(\rho)$ satisfying the first variation conditions are then concisely described by

$$(4.5) \qquad \frac{\delta \mathcal{F}}{\delta \rho}(\rho^*) \left\{ \begin{array}{ll} = -2 & \text{if } \rho^*(\mathbf{x}) > 0, \\ > -2 & \text{if } \rho^*(\mathbf{x}) = 0 \end{array} \right. \implies \rho^*(\mathbf{x}) = \rho^*(\mathbf{x}) \int_{\Omega} \rho^*(\mathbf{x} + \mathbf{y}) \frac{F_R(\mathbf{y})}{F_{\rho^*}(\mathbf{y})} \, \mathrm{d}\mathbf{y}.$$

Equation (4.5) may now be used to devise an iterative fixed-point algorithm.

Recovering $\rho^*(\mathbf{x})$ from $F_R(\mathbf{x})$ (Schulz-Snyder).

- 1. Initialize $\rho_0(\mathbf{x}) > 0$ to be strictly positive with $\int_{\Omega} \rho_0(\mathbf{x}) d\mathbf{x} = 1$. Ensure that $\rho_0(\mathbf{x})$ has no planes of symmetry: For any fixed vector \mathbf{a} , the shifted $\rho_0(\mathbf{x})$ is not even symmetric, $\rho_0(\mathbf{a} \mathbf{x}) \neq \rho_0(\mathbf{x} \mathbf{a})$.
- 2. Iterate the discrete mapping:

$$\rho_{n+1}(\mathbf{x}) = -\frac{1}{2}\rho_n(\mathbf{x})\frac{\delta \mathcal{F}}{\delta \rho}(\rho_n) \qquad \text{for } \mathbf{x} \in \Omega \text{ and } n = 1, 2, 3 \dots$$

$$= \rho_n(\mathbf{x}) \int_{\Omega} \rho_n(\mathbf{x} + \mathbf{y}) \frac{F_R(\mathbf{y})}{F_{\rho_n}(\mathbf{y})} \, \mathrm{d}\mathbf{y},$$
where $F_{\rho_n}(\mathbf{x}) = \rho_n \circ \rho_n$ and we have used the fact that $F_R(\mathbf{y}) = F_R(-\mathbf{y})$.

3. Take $\rho^*(\mathbf{x}) = \rho_{\infty}(\mathbf{x})$ as the candidate global minimizer to (P).

The algorithm also ensures the following properties, which we state without proof:⁶

- 1. (positivity preserving) $\rho_n(\mathbf{x}) \geq 0$ for all \mathbf{x} and $n \geq 0$.
- 2. (mass preserving) $\int_{\Omega} \rho_n(\mathbf{x}) d\mathbf{x} = 1$ for all $n \geq 0$.
- 3. (monotonicity) $\mathcal{F}(\rho_{n+1}) \leq \mathcal{F}(\rho_n)$ for all $n \geq 0$.
- 4. (fixed points) If $\rho^*(\mathbf{x})$ is a fixed point in the Schulz-Snyder algorithm, then $\rho^*(\mathbf{x})$ satisfies the first variation conditions (4.5).

Finally, as prescribed in step 1 of the Schulz-Snyder algorithm, it is important to avoid initializing the data $\rho_0(\mathbf{x})$ to lie in any invariant set of the iterative map from step 2. Initializing the data $\rho_0(\mathbf{x})$ to lie in an invariant set can potentially constrain the resulting fixed-point minimizer $\rho^*(\mathbf{x})$ to have the same symmetry as $\rho_0(\mathbf{x})$. The Schulz-Snyder algorithm has invariant sets that include the following subspaces:

⁶Note: properties 1, 2, and 4 are straightforward to prove. See [50] for a proof of a discrete version of the monotonicity property 3.

- If $\rho_n(\mathbf{x}_p) = 0$ for some point $\mathbf{x}_p \in \Omega$, then $\rho_{n+1}(\mathbf{x}_p) = 0$.
- If for a fixed vector \mathbf{a} , $\rho_n(\mathbf{a} \mathbf{x}) = \rho_n(\mathbf{x} \mathbf{a})$, then $\rho_{n+1}(\mathbf{a} \mathbf{x}) = \rho_{n+1}(\mathbf{x} \mathbf{a})$.

The first symmetry regarding $\rho_{n+1}(\mathbf{x}_p) = 0$ follows directly from testing both sides of step 2 in the iterative scheme at a point $\mathbf{x}_p \in \Omega$. The second property, regarding planes of symmetry, can be shown as well since both $F_R(\mathbf{x})$ and $F_{\rho}(\mathbf{x})$ are mirror symmetric about $\mathbf{0}$:

$$\rho_{n+1}(\mathbf{a} - \mathbf{x}) = \rho_n(\mathbf{a} - \mathbf{x}) \int_{\Omega} \rho_n(\mathbf{a} - \mathbf{x} + \mathbf{y}) \frac{F_R(\mathbf{y})}{F_{\rho_n}(\mathbf{y})} d\mathbf{y}$$

$$= \rho_n(\mathbf{a} - \mathbf{x}) \int_{\Omega} \rho_n(\mathbf{a} - \mathbf{x} - \mathbf{y}) \frac{F_R(\mathbf{y})}{F_{\rho_n}(\mathbf{y})} d\mathbf{y}$$

$$= \rho_n(\mathbf{x} - \mathbf{a}) \int_{\Omega} \rho_n(\mathbf{x} - \mathbf{a} + \mathbf{y}) \frac{F_R(\mathbf{y})}{F_{\rho_n}(\mathbf{y})} d\mathbf{y} = \rho_{n+1}(\mathbf{x} + \mathbf{a}).$$

We now briefly discuss several numerical details of the Schulz-Snyder algorithm. One advantage with minimizing the Kullback-Liebler divergence over other norms or metrics is that the Schulz-Snyder algorithm may be numerically computed using integral quadrature rules, without enforcing nonnegativity and mass constraints. Moreover, up to a negative sign in \mathbf{x} , the integral in step 2 of the algorithm has the form of a convolution—which may also be computed in an efficient manner using the fast Fourier transform. Finally, regarding the convergence rate of the scheme, one might heuristically expect it to behave in a fashion similar to other iterative methods with an exponential convergence at large n, i.e., $|\mathcal{F}(\rho_n) - \mathcal{F}(\rho_\infty)| \sim \gamma^n$ for a value of $0 < \gamma < 1$. Together these properties make using the Kullback-Liebler divergence an attractive approach for practitioners.

In section 2, necessary conditions for a candidate minimizer to solve (P) were given by (2.2), (2.3), and (2.5). Although numerical examples in sections 6 and 7 provide supporting evidence that solutions to (4.5) may (at least in some cases) satisfy (2.2), (2.3), and (2.5), we have no formal proof of such a result. The minimization via the Schultz-Snyder algorithm does, however, often recover candidates $\rho^*(\mathbf{x})$ with $F_{\rho^*}(\mathbf{x})$ having the same support as $F_R(\mathbf{x})$ —which, as we will show through the introduction of the dual formulation to (R), guarantees the necessary condition related to (2.5) in Remark 2.2.

5. The dual decomposition. The purpose of this section is to formulate the dual optimization problem to the convex relation (R), and show how it may be used, in some cases, to explain why the supports of the recovered minimizers $\rho^*(\mathbf{x})$ satisfy the necessary conditions in Remark 2.2. This will be done in two steps. First, the dual formulation will provide a decomposition of the pairwise energy $\mathcal{E}(\rho)$ that takes the form of a nonconvex/convex splitting,

(5.1)
$$\mathcal{E}(\rho) = \mathcal{E}^{+}(\rho) + \mathcal{K}(\rho),$$

where

- 1. $\mathcal{E}^+(\rho) \geq 0$, is a nonnegative functional for all nonnegative measures $\rho(\mathbf{x}) \in \mathcal{C}_1$ and, in general, is nonconvex.
- 2. $\mathcal{K}(f)$ is convex for all finite measures $f(\mathbf{x})$. Namely, for all $0 \le \lambda \le 1$ and $f_1(\mathbf{x}), f_2(\mathbf{x})$ (which may be negative), one has

$$\mathcal{K}(\lambda f_1 + (1 - \lambda)f_2) \le \lambda \mathcal{K}(f_1) + (1 - \lambda)\mathcal{K}(f_2).$$

Second, the nonnegative part of the decomposition (5.1), $\mathcal{E}^+(\rho)$, will be used to provide a sufficient condition to satisfy the necessary conditions in Remark 2.2.

Decompositions of the form given by (5.1) are in general not unique. However, the dual formulation to (R) will provide such a decomposition that also maximizes the minimum value of the convex functional $\mathcal{K}(\rho)$ over probabilities $\rho(\mathbf{x})$. In other words, we will seek $\mathcal{K}(\rho)$ to be, in some sense, the largest convex functional that underestimates $\mathcal{E}(\rho)$. As a result, the optimal functional $\mathcal{K}(\rho)$ that we compute has a strong resemblance to the convex envelope of $\mathcal{E}(\rho)$.

We will show below that an optimal decomposition of the form (5.1) may be formulated as the dual problem to (R)—and therefore computed with the same computational cost as solving (R). Here the construction of the optimal decomposition of the form (5.1) will arise by decomposing the interaction energy $W(\mathbf{x})$ into the sum of a nonnegative function, and a function with nonnegative cosine modes.

To motivate the dual formulation to (R), first consider any decomposition for $W(\mathbf{x})$ that takes the form

(5.2)
$$W(\mathbf{x}) = W^{+}(\mathbf{x}) + K(\mathbf{x}) + 2\mathcal{E}_{D},$$

where

- (D1) $0 \leq W^+(\mathbf{x}) \in \mathcal{C}^0(\Omega)$ is a continuous, nonnegative, mirror symmetric function (see Remark 1.1).
- (D2) $K(\mathbf{x})$ is a continuous, mirror symmetric, mean-zero function with real nonnegative cosine coefficients, i.e.,

$$\hat{K}(\mathbf{k}) := \int_{\Omega} K(\mathbf{x}) \cos(2\pi \mathbf{k} \cdot \mathbf{x}) \, d\mathbf{x} \ge 0 \text{ for all } \mathbf{k} \in \mathbb{Z}^d \setminus \mathbf{0} \text{ and } \hat{K}(\mathbf{0}) = 0,$$

$$K(\mathbf{x}) = \sum_{\mathbf{k} \in \mathbb{Z}^d} \hat{K}(\mathbf{k}) \cos(2\pi \mathbf{k} \cdot \mathbf{x}).$$

Note that the summation in the above cosine series includes all $\mathbf{k} \in \mathbb{Z}^d$, and the inclusion of $\hat{K}(-\mathbf{k}) = \hat{K}(\mathbf{k})$ accounts for the apparent missing factor of 2.

We also make the following technical assumption on the cosine coefficients of $K(\mathbf{x})$:

(5.3)
$$\sum_{\mathbf{k} \in \mathbb{Z}^d} \hat{K}(\mathbf{k}) < \infty.$$

Assumption (5.3) guarantees that the cosine series for $K(\mathbf{x})$ converges uniformly, for instance, by a Weierstrass M-test. Moreover (5.3) will be sufficient to use a Plancherel-type theorem when integrating $K(\mathbf{x})$ against probability measures.

(D3) \mathcal{E}_D is a constant. Due to the normalization convention (W4), of $W(\mathbf{x})$, we see that $\mathcal{E}_D = -\frac{1}{2} \int_{\Omega} W^+(\mathbf{x}) d\mathbf{x}$ will be negative for decompositions of the form (5.2).

Proposition 5.1 (properties of the decomposition (5.2)). Any decomposition of the form (5.2) with properties (D1)–(D3) satisfies the following:

1. The functions $W^+(\mathbf{x})$ and $K(\mathbf{x})$ are in the dual cones to C_1 and C_2 , i.e., $W^+(\mathbf{x}) \in C_1^*$ and $K(\mathbf{x}) \in C_2^*$, where the dual cone X^* to a convex cone X is given by

$$X^* := \{ x \in X' : \langle x, y \rangle > 0, \forall y \in X \}.$$

- 2. $\mathcal{E}_D \leq \mathcal{E}_R$ is a lower bound to (R).
- 3. The following functional is nonnegative:

$$\mathcal{E}^{+}(\rho) := \frac{1}{2} \int_{\Omega} \int_{\Omega} \rho(\mathbf{x}) \rho(\mathbf{y}) W^{+}(\mathbf{x} - \mathbf{y}) \, d\mathbf{x} \, d\mathbf{y} \ge 0 \quad \text{for all } \rho(\mathbf{x}) \in \mathcal{C}_{1}.$$

4. The following functional is convex for $\rho(\mathbf{x}) \in \mathcal{C}_1$:

$$\mathcal{K}(\rho) := \frac{1}{2} \int_{\Omega} \int_{\Omega} \rho(\mathbf{x}) \rho(\mathbf{y}) K(\mathbf{x} - \mathbf{y}) \, d\mathbf{x} \, d\mathbf{y} + \mathcal{E}_{D}.$$

Proof. The proof again involves computing the appropriate integrals.

For 1 we have the following.

- Given $F(\mathbf{x}) \in \mathcal{C}_1$, then $\langle F, W^+ \rangle = \int_{\Omega} W^+(\mathbf{x}) F(\mathbf{x}) d\mathbf{x} \geq 0$, since $W^+(\mathbf{x}) \geq 0$, and $F(\mathbf{x}) \in \mathcal{C}_1$ is nonnegative.
- Given $F(\mathbf{x}) \in \mathcal{C}_2$, then $\langle F, K \rangle = \sum_{\mathbf{k} \in \mathbb{Z}^d} \hat{K}(\mathbf{k}) \hat{F}(\mathbf{k}) \geq 0$, since $\hat{K}(\mathbf{k}) \geq 0$, and $\hat{F}(\mathbf{k}) := \langle F, \cos(2\pi \mathbf{k} \cdot \mathbf{x}) \rangle \geq 0$ for all $\mathbf{k} \in \mathbb{Z}^d$.

Hence $W^+(\mathbf{x})$ and $K(\mathbf{x})$ are in the dual cones to \mathcal{C}_1 and \mathcal{C}_2 , respectively.

For 2, a direct calculations shows

(5.4)
$$\mathcal{E}_{R} = \frac{1}{2} \langle F_{R}, W \rangle$$
$$= \frac{1}{2} \left(\langle F_{R}, W^{+} \rangle + \langle F_{R}, K \rangle \right) + \mathcal{E}_{D} \ge \mathcal{E}_{D}.$$

The last inequality follows since each pairing independently is nonnegative. Namely, $F_R(\mathbf{x})$ is in both C_1 and C_2 and so the result in part 1 applies. Hence, both $\langle F_R, W^+ \rangle \geq 0$ and $\langle F_R, K \rangle \geq 0$.

For 3, the proof is identical to the proof of property (A1) in Proposition 3.1.

For 4: Since $K(\mathbf{x})$ satisfies (5.3), uniform convergence of the cosine series allows one to write $\mathcal{K}(\rho)$ using a Plancherel-type identity. Specifically, for any $\rho(\mathbf{x}) \in \mathcal{C}_1$,

$$\mathcal{K}(\rho) = \frac{1}{2} \sum_{\mathbf{k} \in \mathbb{Z}^d} \hat{K}(\mathbf{k}) \left(\langle \rho, \cos(2\pi \mathbf{k} \cdot \mathbf{x}) \rangle^2 + \langle \rho, \sin(2\pi \mathbf{k} \cdot \mathbf{x}) \rangle^2 \right) + \mathcal{E}_D.$$

Since $\hat{K}(\mathbf{k}) \geq 0$, the functional $\mathcal{K}(\rho)$ is a positive definite quadratic—and hence convex. Note that, in general, numerical observations later show it is often the case that $\hat{K}(\mathbf{k}) = 0$ for some subset of integers \mathbf{k} , indicating that $\mathcal{K}(\rho)$ is not strictly convex.

The dual problem (D) to (R) is then formulated as optimizing (5.2) to find the *best possible* constant \mathcal{E}_D and corresponding decomposition for $W(\mathbf{x})$ into the sum of a nonnegative function and a function with nonnegative cosine modes:

(5.5) (D) Maximize
$$\mathcal{E}_D$$
,
subject to $(W(\mathbf{x}) - 2\mathcal{E}_D) \in \operatorname{cl} (\mathcal{C}_1^* + \mathcal{C}_2^*)$.

⁷Here we provide some details justifying the series expansion for $\langle F, K \rangle$. Note that if $K(\mathbf{x})$ satisfies assumption (5.3), then the cosine series converges uniformly. Hence, for any $\epsilon > 0$, there exists an M > 0, such that $\max_{\mathbf{x} \in [0,1]^d} \|D_M(\mathbf{x})\| < \epsilon$, where $D_M(\mathbf{x}) := K(\mathbf{x}) - \sum_{|\mathbf{k}| < M} \hat{K}(\mathbf{k}) \cos(2\pi \mathbf{k} \cdot \mathbf{x})$. Since $D_M(\mathbf{x})$ is continuous with a maximum norm of ϵ , this implies that $\langle F, D_M \rangle \to 0$ as $M \to \infty$. Hence, $\langle F, K \rangle \to \sum_{\mathbf{k} \in \mathbb{Z}^d} \hat{K}(\mathbf{k}) \hat{F}(\mathbf{k})$ as $M \to \infty$.

Here cl is the weak* closure, $C_{1,2}^*$ are the dual cones⁸ to $C_{1,2}$, where the sum $C_1^* + C_2^* = \{u + v : u \in C_1^*, v \in C_2^*\}$.

Assumption 5.2 (regularity assumption). We assume there exists functions $W_R^+(\mathbf{x}) \in \mathcal{C}_1^*$ and $K_R(\mathbf{x}) \in \mathcal{C}_2^*$ that solve (D), and also satisfy the smoothness properties in (D1)–(D2). In other words, $W(\mathbf{x})$ may be written as an optimal decomposition into the dual cones of \mathcal{C}_1 and \mathcal{C}_2 :

(5.6)
$$W(\mathbf{x}) = W_R^+(\mathbf{x}) + K_R(\mathbf{x}) + 2\mathcal{E}_R,$$

where the optimum value of \mathcal{E}_D in (D) is the same as \mathcal{E}_R .

We refer to the optimal decomposition (5.6) of the interaction energy as the *dual decomposition*, as it arises from the dual formulation of (D) to (R). At the level of numerical discretizations presented in Appendix B, the Assumption 5.2 is justified by the following remark.

Remark 5.3 (numerical justification of Assumption 5.2). Numerical discretizations of (R) presented in Appendix B result in a linear program—which, therefore, has a duality gap of zero. Hence, every numerical discretization of (R) has the optimal value \mathcal{E}_R equal to the optimal value \mathcal{E}_D in (D). Moreover, the finite dimensional cones $\mathcal{C}_{1,h}$ and $\mathcal{C}_{2,h}$ that arise as the discrete approximations to \mathcal{C}_1 and \mathcal{C}_2 are closed, self-dual, and polyhedral. The sum of two polyhedral cones is also polyhedral and hence closed ([47, Theorem 19.1 and Corollary 19.32]). Therefore, for any finite discretization, one has $(\mathcal{C}_{1,h} \cap \mathcal{C}_{2,h})^* = \operatorname{cl}(\mathcal{C}_{1,h}^* + \mathcal{C}_{2,h}^*) = \mathcal{C}_{1,h} + \mathcal{C}_{2,h}$, showing that the dual cone \mathcal{C}_h^* can be written as the sum of the cones $\mathcal{C}_{1,h}$ and $\mathcal{C}_{2,h}$. This justifies, for any finite dimensional discretization, the existence of an optimal dual decomposition of the form (5.6). Note that in general, the sum of two closed, but nonpolyhedral cones, may not be closed. For example, for two closed convex cones $\mathcal{C}_1, \mathcal{C}_2 \subset \mathbb{R}^n$, one may have the pathological situation where a point $\mathbf{x} \in \operatorname{cl}(\mathcal{C}_1 + \mathcal{C}_2)$, however, there are no values $\mathbf{y} \in \mathcal{C}_1$, $\mathbf{z} \in \mathcal{C}_2$ such that $\mathbf{x} = \mathbf{y} + \mathbf{z}$.

With the Assumption 5.2 on the existence of a dual decomposition, the dual problem (D) may be written as a conic optimization problem with linear constraints:

(D) Maximize
$$\mathcal{E}_D$$
,
subject to $(W(\mathbf{x}) - 2\mathcal{E}_D - K(\mathbf{x})) \ge 0$,
 $\langle K, \cos(2\pi \mathbf{k} \cdot \mathbf{x}) \rangle \ge 0$, $\langle K, 1 \rangle = 0$,
 $\langle K, \sin(2\pi \mathbf{k} \cdot \mathbf{x}) \rangle = 0$
for all $\mathbf{x} \in \Omega$ and $\mathbf{k} \in \mathbb{Z}^d \setminus \mathbf{0}$.

Remark 5.4 (regularity observation). The regularity of the optimal decomposition to (D) is an interesting problem: Numerical solutions in dimension one (see section 6) suggest that if W(x) is smooth at x, then $W_R^+(x)$ and $K_R(x)$ are not necessarily smooth at x (although continuity of $W_R^+(x)$ and $K_R(x)$ has been observed).

⁸The formulation (D) is over the dual cone \mathcal{C}^* , which (see Lemma 3.1 in [7] for two intersecting closed convex cones) is equal to $\mathcal{C}^* = (\mathcal{C}_1 \cap \mathcal{C}_2)^* = \operatorname{cl}(\mathcal{C}_1^* + \mathcal{C}_2^*)$.

Remark 5.5 (examples of decompositions for $W(\mathbf{x})$). Two examples of feasible dual decompositions, i.e., of the form in (5.2), are the following.

Example 1: Take $\mathcal{E}_D = \frac{1}{2} \min_{\mathbf{x} \in \Omega} W(\mathbf{x}), K(\mathbf{x}) = 0$, and $W^+(\mathbf{x}) := W(\mathbf{x}) - 2\mathcal{E}_D \ge 0$.

Example 2: Write $W(\mathbf{x}) = K_{+}(\mathbf{x}) + K_{-}(\mathbf{x}) + 2\mathcal{E}_{D}$ as the sum of two functions, where $K_{\pm}(\mathbf{x})$ has only \pm cosine coefficients. Take $K(\mathbf{x}) = K_{+}(\mathbf{x})$ to be the projection of $W(\mathbf{x})$ onto cosine modes with positive coefficients, let $\mathcal{E}_D := \frac{1}{2} \min_{\mathbf{x} \in \Omega} (W(\mathbf{x}) - \mathbf{x})$ $K(\mathbf{x})$, and take $W^+(\mathbf{x}) = W(\mathbf{x}) - K(\mathbf{x}) - 2\mathcal{E}_D \ge 0$.

5.1. Properties of the optimal dual decomposition. The purpose of this subsection is to show that the support of $W_R^+(\mathbf{x})$ can be used to identify sets S_* in which the functional $\mathcal{E}(\rho)$ is convex whenever $\operatorname{supp}(\rho) \subseteq S_*$. Specifically, the conclusion of the subsection will provide a sufficient condition for a candidate minimizer $\rho^*(\mathbf{x})$ to satisfy the necessary condition given in Remark 2.2.

We first discuss the support of $W_R^+(\mathbf{x})$ in relation to $F_R(\mathbf{x})$. Revisiting the lower bound (R) and writing $W(\mathbf{x})$ using the optimal dual decomposition yields

(5.7)
$$\mathcal{E}_R = \frac{1}{2} \langle W, F_R \rangle = \frac{1}{2} \langle W_R^+, F_R \rangle + \frac{1}{2} \langle K_R, F_R \rangle + \mathcal{E}_R.$$

Since both $W_R^+(\mathbf{x}), K_R(\mathbf{x})$ are in the appropriate dual cones, the pairings $\langle W_R^+, F_R \rangle \geq 0$ and $\langle K_R, F_R \rangle \geq 0$. Therefore, (5.7) holds only if the integrals vanish,

$$\langle W_R^+, F_R \rangle = 0, \qquad \langle K_R, F_R \rangle = 0.$$

Here the constraint (5.8) can be used to infer that $F_R(\mathbf{x})$ must have a complementary support to $W_R^+(\mathbf{x})$ in real space, and $K_R(\mathbf{x})$ in \mathbf{k} space. Specifically we have the following cases.

Case 1: When $F_R(\mathbf{x}) \in C^0(\Omega)$ is continuous, the dual decomposition satisfies

(5.9)
$$W_R^+(\mathbf{x})F_R(\mathbf{x}) = 0 \qquad \text{for all } \mathbf{x} \in \Omega,$$

(5.10)
$$\hat{K}_R(\mathbf{k})\hat{F}_R(\mathbf{k}) = 0 \qquad \text{for all } \mathbf{k} \in \mathbb{Z}^d.$$

Here $\hat{F}_R(\mathbf{k})$, $\hat{K}_R(\mathbf{k})$ are the cosine coefficients defined in the proof of Proposition 5.1.

Case 2: When $F_R(\mathbf{x}) = \sum_{\mathbf{r} \in R} f_R(\mathbf{r}) \delta(\mathbf{x} - \mathbf{r})$ is a collection of Dirac masses at the locations $R = {\mathbf{x}_1, \mathbf{x}_2, \dots \mathbf{x}_m}, \text{ with amplitudes } f_R(\mathbf{r}),$

$$(5.11) W_R^+(\mathbf{r}) = 0 \text{for all } \mathbf{r} \in R,$$

(5.11)
$$W_R^+(\mathbf{r}) = 0 \qquad \text{for all } \mathbf{r} \in R,$$
(5.12)
$$\hat{K}_R(\mathbf{k})\hat{F}_R(\mathbf{k}) = 0 \qquad \text{for all } \mathbf{k} \in \mathbb{Z}^d.$$

Again $\hat{K}_R(\mathbf{k})$ and $\hat{F}_R(\mathbf{k})$ are the cosine coefficients of $K_R(\mathbf{x})$ and $F_R(\mathbf{x})$, where $F_R(\mathbf{k})$ can be expressed in terms of $f_R(\mathbf{r})$:

$$\hat{F}_R(\mathbf{k}) = \langle F_R, \cos(2\pi \mathbf{k} \cdot \mathbf{x}) \rangle = \sum_{\mathbf{r} \in R} f_R(\mathbf{r}) \cos(2\pi \mathbf{k} \cdot \mathbf{r}).$$

Equation (5.9) (or the discrete version of (5.11)) shows that $W_R^+(\mathbf{x}) = 0$ whenever $F_R(\mathbf{x}) \neq 0$, and vice versa. We now combine this observation with the results from Proposition 5.1. First set

$$\mathcal{E}_{R}^{+}(\rho) := \frac{1}{2} \int_{\Omega} \int_{\Omega} \rho(\mathbf{x}) \rho(\mathbf{y}) W_{R}^{+}(\mathbf{x} - \mathbf{y}) \, d\mathbf{x} \, d\mathbf{y} = \frac{1}{2} \langle \rho \circ \rho, W_{R}^{+} \rangle,$$

$$\mathcal{K}_{R}(\rho) := \frac{1}{2} \int_{\Omega} \int_{\Omega} \rho(\mathbf{x}) \rho(\mathbf{y}) K_{R}(\mathbf{x} - \mathbf{y}) \, d\mathbf{x} \, d\mathbf{y} + \mathcal{E}_{R},$$

where $\mathcal{E}(\rho) = \mathcal{E}_R^+(\rho) + \mathcal{K}_R(\rho)$ is the functional decomposition for $\mathcal{E}(\rho)$ that arises from the optimal dual decomposition. We now arrive at the main observation.

Proposition 5.6 (sets where $\mathcal{E}(\rho)$ is convex). Consider a candidate minimizer $\rho^*(\mathbf{x})$ with support S_* , and suppose that the support of $F_{\rho}(\mathbf{x}) = \rho^* \circ \rho^*$ lies in the support of $F_R(\mathbf{x})$, i.e., $\operatorname{supp}(\rho^* \circ \rho^*) \subseteq \operatorname{supp}(F_R)$. Then $\mathcal{E}(\rho)$ is convex on the space of probabilities having support S_* . In other words, $\mathcal{E}(\rho)$ is convex when restricted to the set

$$\mathcal{B}_* := \left\{ \rho(\mathbf{x}) \in \mathcal{C}_1, \int_{\Omega} \rho(\mathbf{x}) \, \mathrm{d}\mathbf{x} = 1, \, \operatorname{supp}(\rho) \subseteq S_* \right\}.$$

Proof. The proof uses the dual decomposition and the complementary support equations (5.9) or (5.11). It will be sufficient to show that for any $\rho(\mathbf{x}) \in \mathcal{B}_*$, we have $\mathcal{E}_R^+(\rho) = 0$. This will imply that on the space \mathcal{B}_* , the functional $\mathcal{E}(\rho) = \mathcal{K}_R(\rho)$ is convex.

Suppose that $\rho(\mathbf{x}) \in \mathcal{B}_*$, then $\operatorname{supp}(\rho \circ \rho) \subseteq \operatorname{supp}(\rho^* \circ \rho^*)$ by a basic property of the auto-correlation of probabilities. Using the hypothesis in Proposition 5.6, one then has that $\operatorname{supp}(\rho \circ \rho) \subseteq \operatorname{supp}(F_R)$. However (5.9) or (5.11) guarantees that $W_R^+(\mathbf{x}) = 0$ for any $\mathbf{x} \in \operatorname{supp}(F_R)$, and hence $W_R^+(\mathbf{x}) = 0$ for any $\mathbf{x} \in \operatorname{supp}(\rho \circ \rho)$. Therefore the integral $\mathcal{E}_R^+(\rho) = \frac{1}{2} \langle \rho \circ \rho, W_R^+ \rangle = 0$.

Proposition 5.1 shows that if a recovered minimizer $\rho^*(\mathbf{x})$ has an auto-correlation with support supp $(F_{\rho}) \subseteq \text{supp}(F_R)$, then $\rho^*(\mathbf{x})$ satisfies the necessary condition for a candidate minimizer outlined in Remark 2.2. In the subsequent numerical examples, we will observe that the recovery procedure outlined in section 4 will generate candidate minimizers $\rho^*(\mathbf{x})$ that often satisfy the hypothesis in Proposition 5.6

Finally, we conclude this section with the observation that finding analytic descriptions for sets S_* in which the energy functional $\mathcal{E}(\rho)$, when restricted to $\rho(\mathbf{x})$ with $\operatorname{supp}(\rho) \subseteq S_*$, is convex is not a simple problem. The importance of the dual decomposition for $W(\mathbf{x})$ is that it is a constructive approach that allows one to find such sets S_* . Specifically, $W_R^+(\mathbf{x})$ and $K_R(\mathbf{x})$ are constructed analytically from $W(\mathbf{x})$; and if a set S_* satisfies the property that $\operatorname{supp}(\rho) \subseteq S_*$ implies $\mathcal{E}_R^+(\rho) = 0$, then $\mathcal{E}(\rho)$ is convex when restricted to probabilities with supports in S_* .

6. Results: Examples in one dimension.

6.1. The Morse potential. In this section we use the convex relaxation and recovery approach to generate candidate minimizers to the Morse potential on a periodic domain. The Morse potential is a simple example of an attractive-repulsive potential that has been used recently [5, 33, 40] to model swarms and collective behavior in social phenomena. On $\Omega = \mathbb{R}$, we write the Morse potential as

(6.1)
$$W_M(x) = -GLe^{-|x|/l_1} + e^{-|x|/l_2}, \qquad G, L > 0, \quad x \in \mathbb{R},$$

where $L := l_1/l_2$ is a dimensionless quantity; l_1 and l_2 are the length scales associated with an attractive and repulsive force, respectively; and G denotes the strength of the attractive part of the potential. Mathematically, for different strengths of attraction and repulsion, the Morse potential results in a nonconvex energy functional $\mathcal{E}(\rho)$. For computational purposes, we work on a periodic domain. To make $W_M(x)$ periodic, we introduce a box size l_{box} , and define the periodic Morse potential as

(6.2)
$$W_{PM}(x) = \sum_{n \in \mathbb{Z}} W_M(x + nl_{box}).$$

Equation (6.2) can then be summed exactly by converting it into a geometric series. To nondimensionalize $W_{PM}(x)$, we use l_{box} as the length scale, and replace $x \to x/l_{box}$. We also introduce the dimensionless parameter $\sigma := l_2/l_{box}$. After summation and nondimensionalization, the function $W_{PM}(x)$, when restricted to one period $0 \le x \le 1$, takes the form

(6.3)
$$W_{PM}(x) = \frac{-GL}{1 - e^{-1/(L\sigma)}} \left(e^{-x/(L\sigma)} + e^{-(1-x)/(L\sigma)} \right) + \frac{1}{1 - e^{-1/\sigma}} \left(e^{-x/\sigma} + e^{-(1-x)/\sigma} \right) - \overline{W}.$$

Here \overline{W} is a constant⁹ added for numerical purposes to normalize $W_{PM}(x)$ to have mean zero (see property (W4)). When the box size $l_{box} \gg l_1, l_2$ is much larger than the interaction length scales, the periodic effects of $W_{PM}(x)$ are expected to be small, and minimizers of $\mathcal{E}(\rho)$ with $W_{PM}(x)$ are expected to recover the results of minimizing $W_{M}(x)$ on the infinite line \mathbb{R} .

In the following numerical examples we fix $\sigma = 0.1$, so that l_{box} is several times larger than l_1 and l_2 . To illustrate the utility of the new approach, we compute the phase diagram for $W_{PM}(x)$ and characterize the results in the (L,G) parameter plane. This is done by systematically computing the minimizer $F_R(x)$ and recovered $\rho^*(x)$ for every value of (L,G). We find that the qualitative properties, which are characterized by four different regions, A–D, in Figure 2 are in agreement with the ones computed in [33]. In particular, the region D corresponds to the blowup region observed in [33]. Within this region, we observe a cascade where minimizers form lattices of Dirac masses—with progressively smaller lattice spacings, as G decreases at a fixed value of L.

Figures 3–5 show explicit results for a fixed value of (L, G) = (1.2, 0.9), that lies in the region where $F_R(x)$ is a continuous function. Figure 3 demonstrates the convergence of the Schulz–Snyder algorithm, while Figure 4 shows the optimal dual decomposition for $W_{PM}(x)$.

Figure 5 altogether shows the recovered minimizer $\rho^*(x)$ (with a guarantee $\alpha = 0.99$), along with the solutions to (R) and (D), i.e., $F_R(x), W_R^+(x), K_R(x)$. The purpose of showing the solutions both to (R) and (D) is to highlight the complementarity conditions (5.9)–(5.10). Specifically, Figure 5(a) shows $\rho^*(x)$ to have a support S_* with length $|S_*| = 0.161$, which is consistent with the histogram width observed in the particle simulations in Figure 1. The autocorrelation $F_\rho(x)$ also has a support supp $(F_\rho) = \sup(F_R)$, and, therefore is complementary to $W_R^+(x)$, i.e., $W_R^+(x)F_\rho(x) = 0$ for all $x \in \Omega$ (See Figure 5(b)). Hence, $\rho^*(x)$ satisfies the hypothesis in Proposition 5.6, which implies that $\mathcal{E}(\rho)$ is convex when restricted to probabilities

$$^{9} \overline{W} = \frac{-GL}{1 - e^{-1/(L\sigma)}} A + \frac{1}{1 - e^{-1/\sigma}} B$$
, where $A = \int_0^1 e^{-x/(L\sigma)} + e^{-(1-x)/(L\sigma)} dx$, and $B = \int_0^1 e^{-x/\sigma} + e^{-(1-x)/\sigma} dx$.

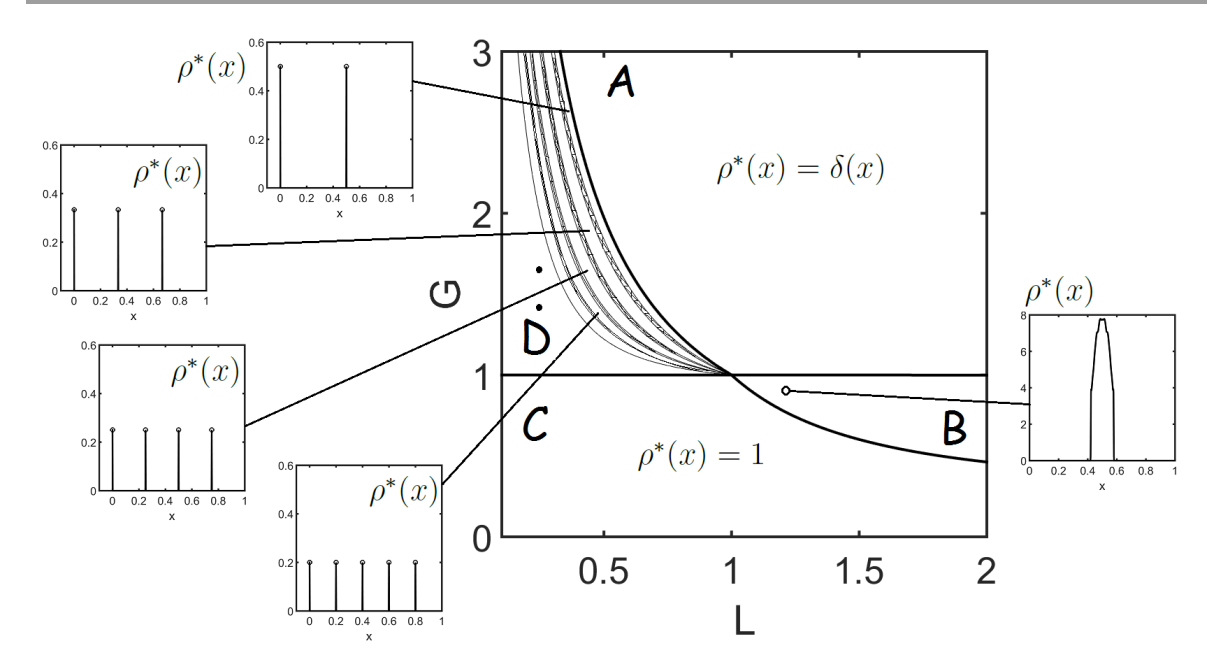


Figure 2. The phase diagram for the periodic Morse potential (6.3) with $\sigma = 0.1$. The (L,G) plane is partitioned by thick black lines into 4 regions, denoted by A–D, which show qualitatively different minimizers $\rho^*(x)$ (Note that these regions are similar to the ones observed in [33].) Region A: The global minimum is $\rho^*(x) = \delta(x)$. Region B: Densities $\rho^*(x)$ have a nonzero width whose support is contained strictly inside [0,1]; and have a continuous auto-correlation $F_R(x)$. Here, one recovered solution is shown for the parameter values (L,G) = (1.2,0.9). Region C: $\rho^*(x) = 1$ corresponds to an evenly spread probability distribution. Region D: Solutions are a collection of Dirac masses, and may form lattices. For instance, the white banded regions show a cascade of lattice minimizers. Plotted are lattices with 2,3,4, and 5 evenly spaced Dirac $\delta(x)$'s, and the number continues to increase as G approaches 1. The small transition regions (black shading), between the lattice regions, may contain (possibly infinitely) many different solutions. Minimizers in regions A, C, as well as the lattice solutions in D are exact global minimizers with $\alpha = 1$ (see Remark 3.6 and Appendix A).

having support with a width of ~ 0.161 . Figure 5(c), shows the complementarity condition (5.10). Finally, we note that the size $|S_*|$ emerges as a new length scale for the particle density, and is exactly 1/2 of the length where $W_R^+(x) = 0$.

6.2. A local potential. In the context of social interactions, recent work [41] has focused on a class of local interaction potentials where W(x) has compact support. In this section we examine the approximate global minimizers and dual decomposition for a continuous periodic version of the local potential examined in [41]:

(6.4)
$$\psi(x) = \begin{cases} 0.1, & |x| \le \frac{1}{2}, \\ 9|x| - 4.4, & \frac{1}{2} < |x| \le \frac{3}{5}, \\ 1, & \frac{3}{5} < |x| \le \frac{9}{10}, \\ 10 - 10|x|, & \frac{9}{10} < |x| \le 1, \\ 0, & |x| > 1, \end{cases}$$
 for $x \in \mathbb{R}$,
$$W(x) = \sum_{n \in \mathbb{Z}} \left(\psi\left(\frac{x+n}{l_c}\right) - \overline{\psi} \right).$$

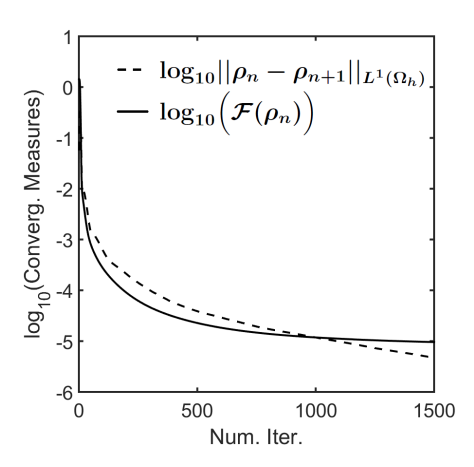


Figure 3. Convergence versus iteration for $\log_{10} \| \rho_n - \rho_{n+1} \|_{L^1(\Omega_h)}$ (dashed curve), and $\log_{10}(\mathcal{F}(\rho_n)) \to 7.98 \times 10^{-6}$ (solid line) in the Schulz-Snyder algorithm. The quantities are for the periodic Morse potential (6.3) with $\sigma = 0.1$, (L, G) = (1.2, 0.9), and grid n = 800. The nonzero value of 7.98×10^{-6} is the result of a mismatch between the converged $F_{\rho^*}(x)$, and target $F_R(x)$, and may be due to (i) round-off or tolerance errors introduced into the numerical discretizations or (ii) a fundamental limitation that for the analytic solution $F_R(x)$ at hand, there may not exist a $\rho^*(x)$ that exactly satisfies the sufficient conditions in Remark 4.1.

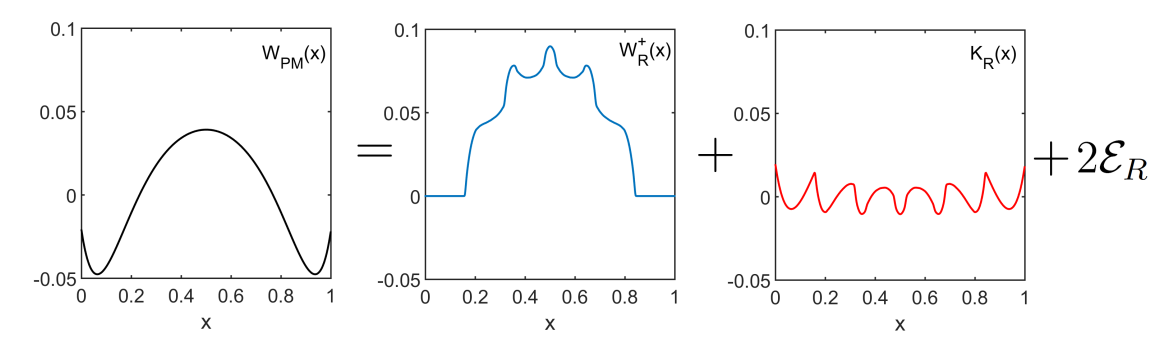


Figure 4. The figure shows the optimal dual decomposition (5.6) for the periodic Morse potential $W_{PM}(x)$ defined in (6.3). Here the parameters are $\sigma = 0.1$, (L, G) = (1.2, 0.9), and grid n = 800. Note that the cosine coefficients of $K_R(x)$ are nonnegative, while \mathcal{E}_R is the largest possible constant as described by the solution to (D).

Figure 6(c) shows the potential $\psi(x)$, which differs primarily from the one in [41] by replacing the discontinuous jumps (at range values 0.1, 1, and 0) by linear interpolation. The quantity $l_c > 0$ enters as the (dimensionless) ratio of the local interaction length to periodic domain length, with W(x) entering in as a full periodic potential. One might expect in the limit $l_c \ll 1$ to recover the characteristics of the nonperiodic model. For $l_c = 0.1$, which is commensurate with the periodic domain length, and n = 360 grid points, one recovers the auto-correlation with 10 equispaced Dirac masses:

(6.5)
$$F_R(x) = \sum_{s \in S} f_R(s)\delta(x - s),$$

$$f_R(s) = \frac{1}{10}, \text{ where } S = \left\{0, \frac{1}{10}, \frac{2}{10}, \dots, \frac{9}{10}\right\}.$$

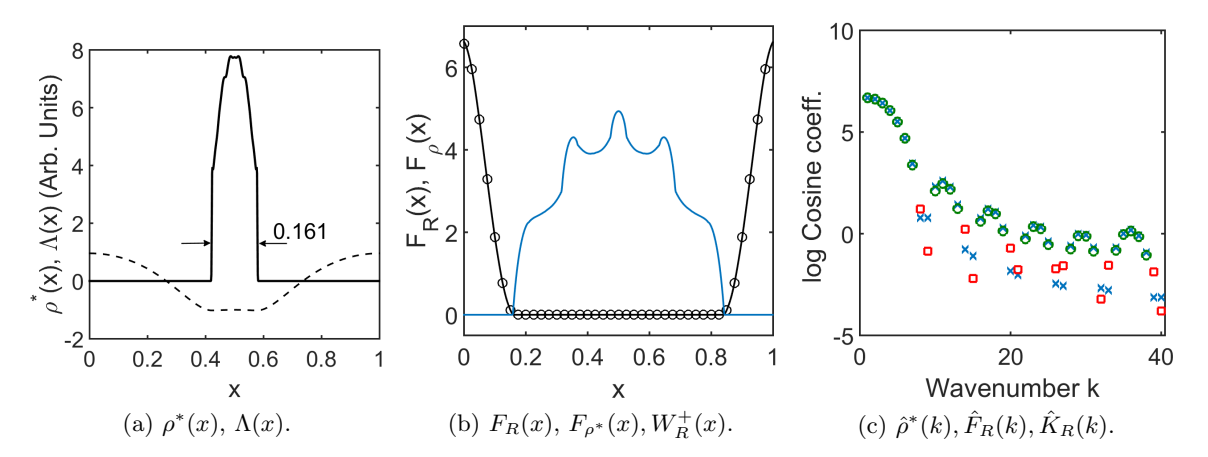


Figure 5. Example for the Morse potential (6.3) with $\sigma = 0.1$, (L,G) = (1.2,0.9), and grid n = 800. (a) shows the recovered minimizer $\rho^*(x)$ (solid curve), which has a guarantee of $\alpha = 0.99$, along with $\Lambda(x)$ (dashed curve, arbitrary units). The width of the support of $\rho^*(x)$ is ~ 0.161 . (b) shows the auto-correlation $F_{\rho^*}(x)$ (solid line), target auto-correlation $F_R(x)$ (circles), and a rescaled $W_R^+(x)$ (blue curve). Here $W_R^+(x)$ is drawn to show that $F_{\rho}(x)$ and $W_R^+(x)$ have complementary supports, i.e., $W_R^+(x)F_{\rho}(x) = 0$. This implies that $\rho^*(x)$ satisfies the hypothesis in Proposition 5.6 and, therefore, $\mathcal{E}(\rho)$ is convex when restricted to probabilities with a width ~ 0.161 . (c) shows that the cosine coefficients (coefficients not plotted are numerically zero) $\hat{F}_R(k)$ (green circles), and $\hat{K}_R(k)$ (red squares), have complementary support for different values of k, i.e., $\hat{F}_R(k)\hat{K}_R(k) = 0$. Here the cosine coefficients $\hat{F}_{\rho^*}(k)$ (blue crosses) of the recovered solution are shown for reference.

Since $F_R(x) = F_R \circ F_R$, letting $\rho^*(x) = F_R(x)$ recovers the exact auto-correlation and hence is a global minimizer with guarantee $\alpha = 1$. Figure 6(a) shows the dual decomposition of $W(x) = W_R^+(x) + K_R(x) + 2\mathcal{E}_R$. Numerically, it is observed that both $W_R^+(x)$ and $K_R(x)$ are constant in regions where the local potential W(x) = 0, so that they too are effectively local potentials. As a final remark, if l_c is not taken as an integer fraction of the domain length, or the grid spacing h = 1/n (see Appendix B) is not commensurate with the spacing of the Dirac masses, one may have nonlattice minimizers that become sensitive to the number of grid points n, and tolerance chosen in the numerical optimization routine.

6.3. A regularized power law potential. Power law potentials are often used in models of social dynamics. Here we illustrate the approach for a regularized power law potential on a periodic domain. Set

$$W_p(x) = x^{-0.4} - \frac{1}{3.5}x^{-0.2} - \overline{W},$$

$$(6.6) W(x) = W_p(x+\epsilon) + W_p(1-x+\epsilon) for x \in [0,1], extended periodically.$$

The exponents -0.4, -0.2 and parameter 3.5 are chosen arbitrarily. The parameter $\epsilon = 0.01$ is taken to regularize the discontinuity at x = 0. Without the regularization, the value W(0) becomes undefined and the optimization routine in Appendix B must be modified to obtain a convergent minimizer to (R). As a note, the shape of the potential is somewhat sensitive to the parameters ϵ and deviations from the constant 3.5. The candidate minimizer $\rho^*(x)$ is shown in Figure 7 and has a guarantee $\alpha = 0.988$.

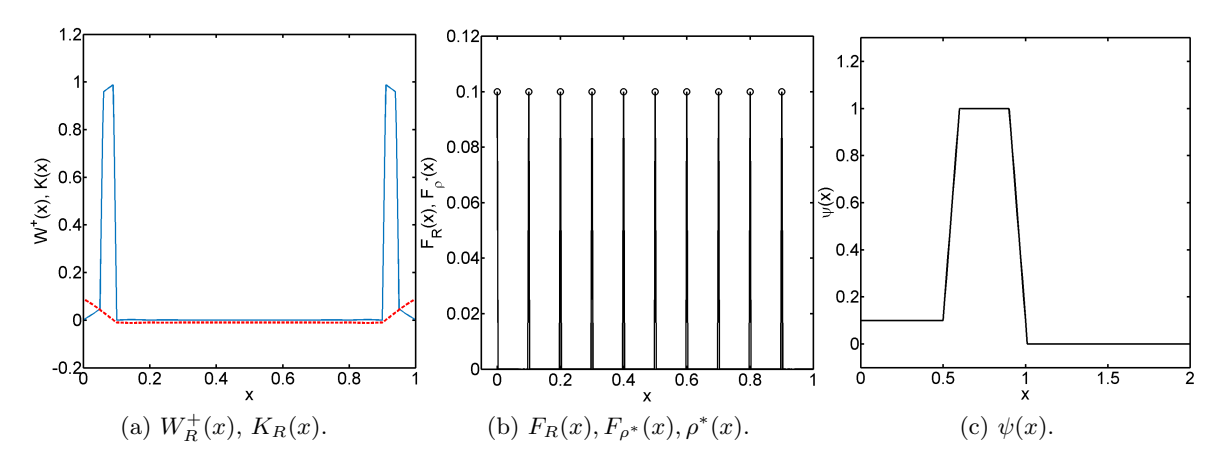


Figure 6. Results for local potential (6.4), n = 360 grid. (a) Optimal dual decomposition for W(x) into $W_R^+(x)$ (blue curve), and $K_R(x)$ (red curve). (b) $F_R(x)$ (circles), $F_{\rho^*}(x) = \rho_*(x)$ (solid lines). The recovery is exact with $\alpha = 1$. (c) Local interaction potential $\psi(x)$.

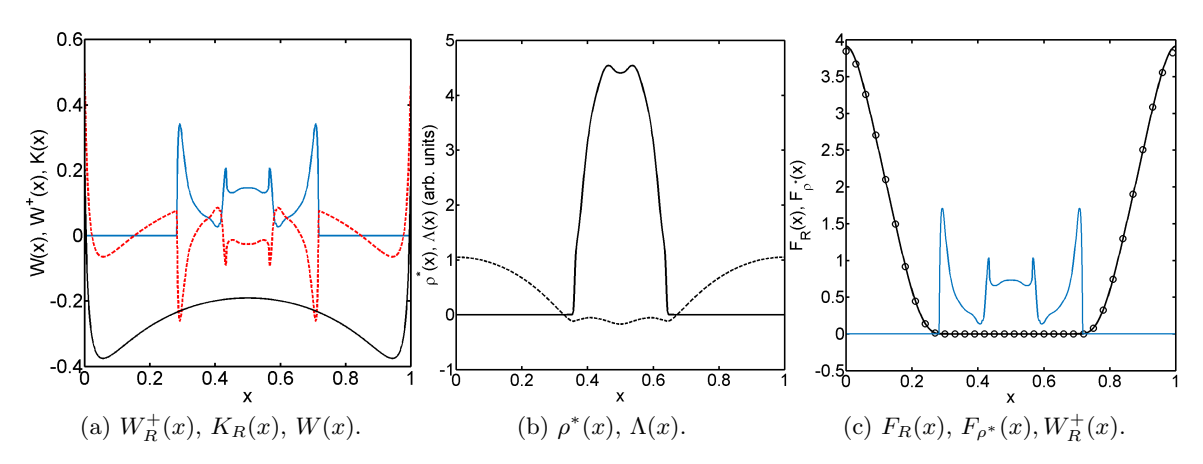


Figure 7. Results for regularized power law potential (6.6), n = 1000 grid. (a) Optimal dual decomposition for W(x) (black curve) into $W_R^+(x)$ (blue curve), and $K_R(x)$ (red curve). (b) $\rho^*(x)$ (solid) with guarantee $\alpha = 0.988$, rescaled $\Lambda(x)$ (dashed) with arbitrary units. (c) Auto-correlation $F_R(x)$ (dots), and $F_{\rho^*}(x)$ (solid). Here $W_R^+(x)$ is plotted (blue curve, arbitrary units) to show that $F_\rho(x)W_R^+(x) = 0$, thereby implying that $\rho^*(x)$ satisfies the hypothesis in Proposition 5.6.

6.4. A potential with multiple length scales. Another interesting example occurs for potentials that promote several length scales by having multiple local minima in W(x). As an example, take

$$W_t(x) = \max\{1 - x, 0\} - \overline{W} \qquad \text{for } x \in [0, 1],$$

$$(6.7) \quad W(x) = W_t\left(\frac{x}{10}\right) + W_t\left(\frac{1 - x}{10}\right) - \frac{1}{2}\cos(4\pi x) \quad \text{for } x \in [0, 1], \text{ extended periodically.}$$

Here $W_t(x)$ is a repulsive triangle potential which has nonnegative cosine modes. The $\cos(4\pi x)$ term is added to make $\mathcal{E}(\rho)$ nonconvex. We find a candidate minimizer $\rho^*(x)$ with a guarantee

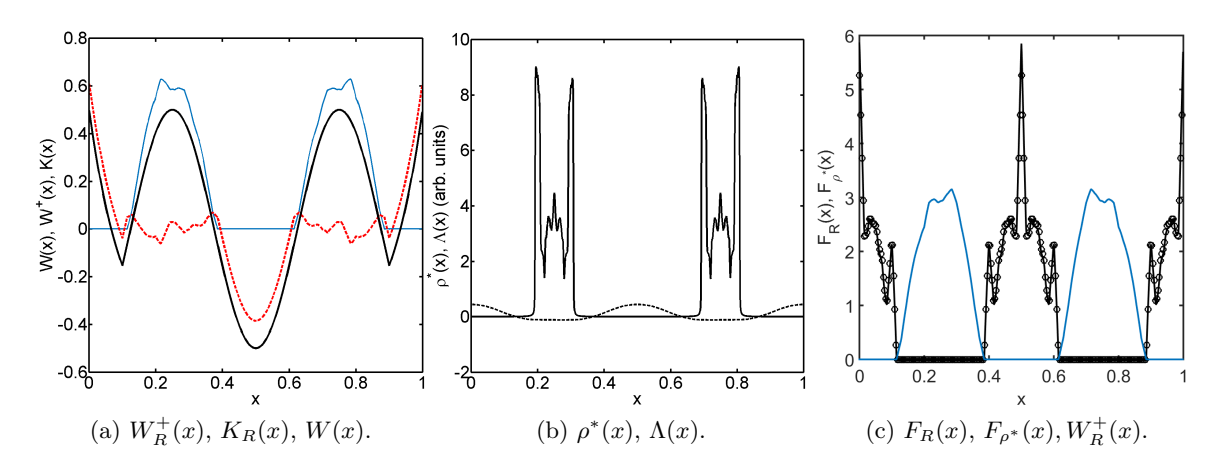


Figure 8. Results for potential with multiple length scales (6.7), n = 1024 grid. (a) Optimal dual decomposition for W(x) (black curve) into $W_R^+(x)$ (blue curve), and $K_R(x)$ (red curve). (b) $\rho^*(x)$ (solid) with guarantee $\alpha = 0.988$, rescaled $\Lambda(x)$ (dashed) with arbitrary units. (c) Auto-correlation $F_R(x)$ (dots), and $F_{\rho^*}(x)$ (solid). Here $W_R^+(x)$ is plotted (blue curve, arbitrary units) to show that $F_\rho(x)W_R^+(x) = 0$, thereby implying that $\rho^*(x)$ satisfies the hypothesis in Proposition 5.6.

 $\alpha = 0.988$ (see Figure 8). The dual decomposition solution found in Figure 8(a) also highlights the fact that $K_R(x)$ and $W_R^+(x)$ are not, in general, smooth.

Remark 6.1 (minimizers with disconnected supports). Other works, such as [5] have been successful in characterizing global minimizers under the assumption that $\rho^*(x)$ has connected support. The recovery process for potential (6.7) yields an $F_R(x)$ with disconnected support, thereby resulting in $\rho^*(x)$ with multiply connected supports.

7. Results: Examples in two dimensions. The purpose of this section is to solve the relaxation (R), and compute minimizers in some examples with two spatial dimensions. The examples will also highlight several difficulties and drawbacks that become more significant in higher dimensions. Specifically, due to the enlarged set of constraints encountered in two dimensions, the numerical solution using the MATLAB solver becomes slow, and motivates the need for more efficient numerical schemes.

Here, we focus on an attractive-repulsive potential that shares some similarity to the periodic Morse potential:

(7.1)
$$W(x,y) = -GLe^{-\frac{1}{L}(|\sin(\pi x)| + |\sin(\pi y)|)} + e^{-(|\sin(\pi x)| + |\sin(\pi y)|)} - \overline{W}, \qquad G, L > 0, \quad x, y \in \mathbb{R}.$$

As a result of the similar parameterization to $W_{PM}(x)$, we may expect minimizers with the potential (7.1) for different G and L values to have qualitatively similar behavior to those described in the phase diagram in Figure 2. For different fixed values of (L, G), we solve (R) for $F_R(\mathbf{x})$, followed by performing the recovery procedure outline in section 4.

7.1. Solutions $F_R(x)$ to (R) that are continuous. Using values of (L, G) = (1.5, 0.9) in (7.1), we obtained a solution $F_R(\mathbf{x})$ that is continuous, as seen in Figure 9(a). In the numerical solution, we were limited to a coarse 40×40 grid due to the increased solution times required

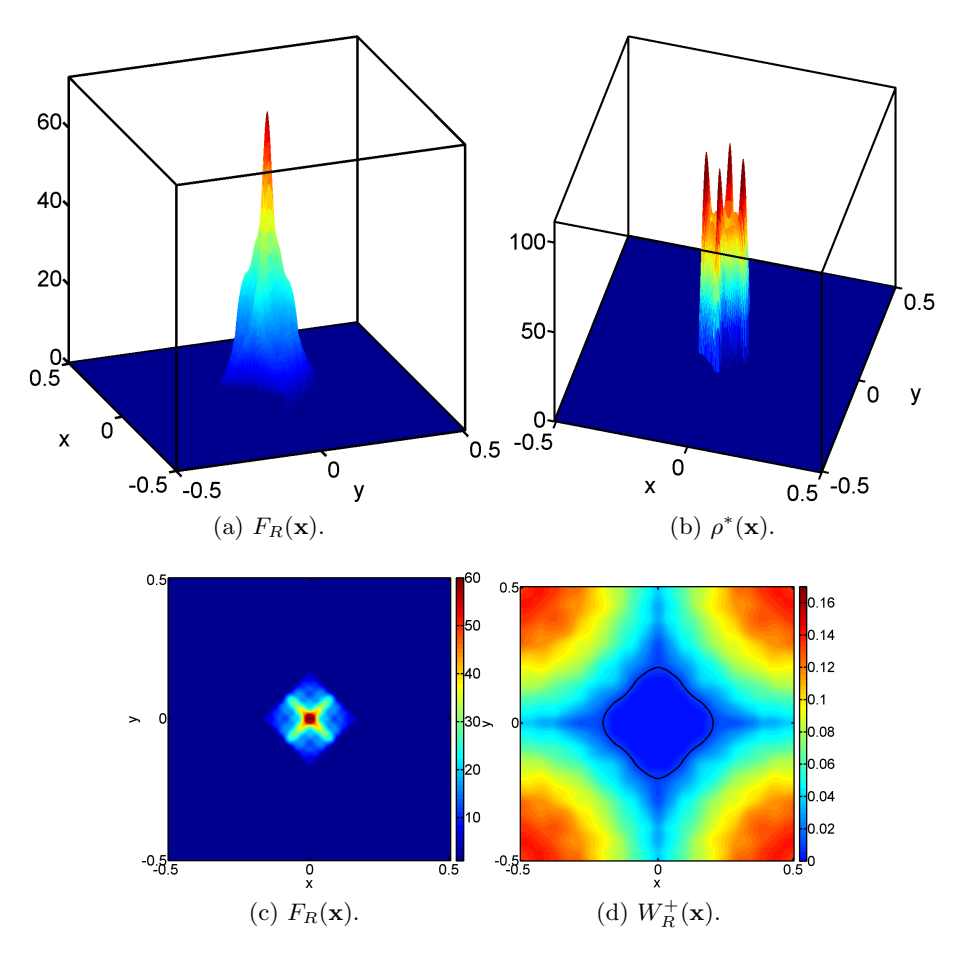


Figure 9. Results for the two dimensional periodic potential in (7.1) with (L, G) = (1.5, 0.9), and 40×40 grid. (a) Target auto-correlation $F_R(\mathbf{x})$. (b) $\rho^*(\mathbf{x})$ with guarantee $\alpha = 0.99$. (c) Contour plot for $F_R(\mathbf{x})$ showing the support. (d) Contour plot of $W_R^+(\mathbf{x})$ with a black line indicating the region where $W_R^+(\mathbf{x}) = 0$. Note that $W_R^+(\mathbf{x})F_\rho(\mathbf{x}) = 0$, implying that $\rho^*(\mathbf{x})$ satisfies Proposition 5.6.

by the MATLAB solvers. In future work we plan to increase the efficiency of the solvers so that larger spatial discretizations may be used. Despite the relatively coarse mesh, we still resolved a numerical solution to $F_R(\mathbf{x})$, which likely has an error to the true solution that is first order, i.e., $\mathcal{O}(1/n)$. We also set the built-in MATLAB tolerance to 10^{-8} . The recovered candidate $\rho^*(\mathbf{x})$ (see Figure 9) was found to have a guarantee of $\alpha = 0.99$, and a relative entropy to $F_R(\mathbf{x})$ of $\mathcal{F}(\rho^*) = 0.0011$. We now make several remarks on the characteristics of $\rho^*(\mathbf{x})$:

- (i) The support of $F_{\rho}(\mathbf{x})$ is complementary to $W_{R}^{+}(\mathbf{x})$, i.e., $F_{\rho}(\mathbf{x})W_{R}^{+}(\mathbf{x}) = 0$. This implies that $\rho^{*}(\mathbf{x})$ satisfies Proposition 5.6 and, hence, $\mathcal{E}(\rho)$ is convex when restricted to densities having a support contained in the support of $\rho^{*}(\mathbf{x})$.
- (ii) The solution $\rho^*(\mathbf{x})$ with support S_* , exhibits spikes at the four corners of the support. To provide some explanation for the spikes, note that the previous item (i) implies that $\mathcal{E}(\rho^*) = \mathcal{K}_R(\rho^*)$ (see also Proposition 5.6). The spikes may then be attributed to the recovered solution $\rho^*(\mathbf{x})$ wanting to minimizing the convex part of the energy $\mathcal{K}_R(\rho)$

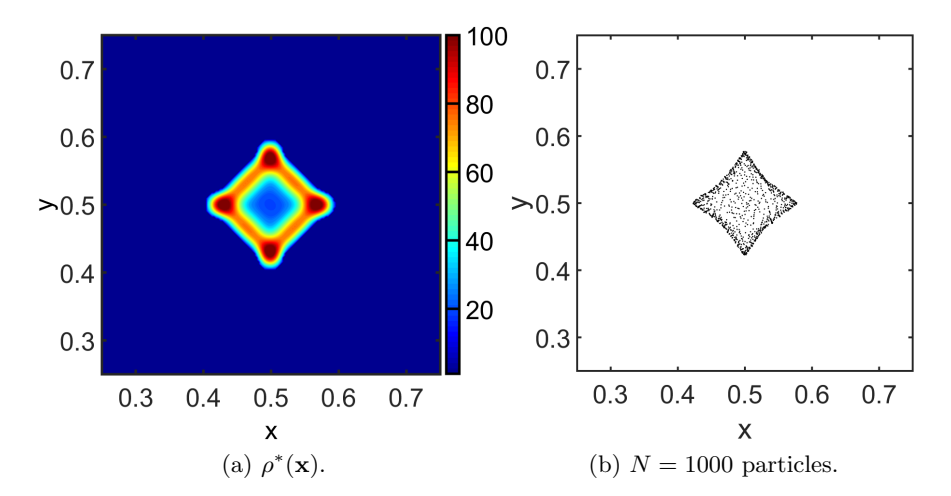


Figure 10. A comparison of the recovered solution $\rho^*(\mathbf{x})$ for the two dimensional periodic potential in (7.1) (for parameters (L,G)=(1.5,0.9), and 40×40 grid); with a discrete steady state gradient flow. (a) shows the contour plot of $\rho^*(x)$, while (b) shows the steady state solution of (1.6) with N=1000 particles. Note the similarity in the support of $\rho^*(x)$ with the coalescence of the individual particles.

that arises from an interaction potential $K_R(\mathbf{x})$. For this example $W_R^+(\mathbf{x}) = 0$ in a diamond neighborhood near the origin, so that within this region $K_R(\mathbf{x}) = W(\mathbf{x}) - 2\mathcal{E}_R$ contains the attractive-repulsive behavior of $W(\mathbf{x})$. Hence, $\rho^*(\mathbf{x})$ can be thought of as a density that arises from locally repelling particles confined to the set S_* . As a result, the majority of the density concentrates near the boundary and corners of S_* .

- (iii) Figure 10 shows the support of the recovered minimizer $\rho^*(\mathbf{x})$, and the steady state arrangement of N = 1000 particles obtained from the gradient flow of (1.6) (using random initial data). The recovered minimizer identifies the emergent length scale and pattern obtained by the collective interaction of a large number of particles.
- **7.2.** Solutions $F_R(x)$ to (R) that are nonclassical. For values of (L,G)=(0.5,1.5), the solution $F_R(\mathbf{x})$ is a collection of discrete Dirac masses. Figure 11 shows the support of $F_R(\mathbf{x})$, $F_{\rho^*}(\mathbf{x})$, and $\rho^*(\mathbf{x})$. As is evident by the small dots in Figure 11(c), this is a case where the recovered $\rho^*(\mathbf{x})$ has an auto-correlation $F_{\rho}(\mathbf{x})$ that is not exactly inside $F_{R}(\mathbf{x})$, i.e., $\operatorname{supp}(F_{\rho}) \nsubseteq \operatorname{supp}(F_R)$. This implies that Proposition 5.6 does not hold, and the recovered minimizer from $F_R(\mathbf{x})$ is only an approximate one at best. One interesting observation is that the recovery procedure successfully matches 93% of the support of $F_{\rho^*}(\mathbf{x})$ with $F_R(\mathbf{x})$, so that $\rho^*(\mathbf{x})$ contains length scales that try to optimize the overall energy $\mathcal{E}(\rho)$. However relative to the constant state $\rho(\mathbf{x}) = 1$, the guarantee is $\alpha = 0.54$, indicating there is a large gap between $\mathcal{E}(\rho^*)$ and the lower bound \mathcal{E}_R . For this example, it is possible that even the true global minimum $\rho_0(\mathbf{x})$ still has a large gap relative to the bound \mathcal{E}_R . Figure 12 compares the support of $\rho^*(\mathbf{x})$ with the steady state arrangement of N=1000 particles obtained from the gradient flow of (1.6) (using random initial data). The figure shows that particles coalesce into points that are not in a well-defined pattern. Finally, we remark that when the recovered minimizers $\rho^*(\mathbf{x})$ have sharp spikes, the exact height and symmetry of the spikes obtained from the Schultz-Snyder algorithm may become sensitive to small perturbations in the target

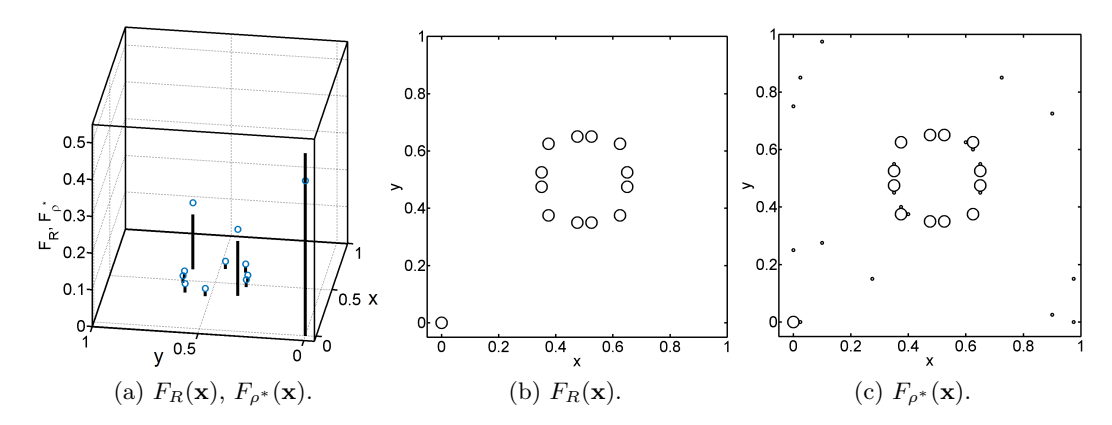


Figure 11. Results for the two dimensional potential in (7.1) with (L,G) = (0.5, 1.5) and a 40×40 grid. (a) shows $F_R(\mathbf{x})$ (black lines) and the recovered $F_{\rho^*}(\mathbf{x})$ (blue circles). (b) shows the support of $F_R(\mathbf{x})$, while (c) shows the support of $F_{\rho^*}(\mathbf{x})$. The large circles account for a total mass of 0.9267, while the small circles (each with mass < 0.006) account for the remaining mass. The value of the functional $\mathcal{F}(\rho^*) = 0.086$.

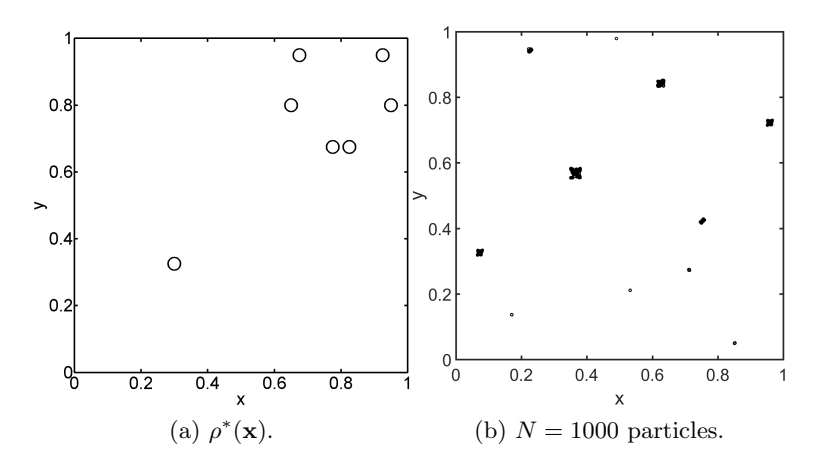


Figure 12. A comparison of the recovered solution $\rho^*(\mathbf{x})$ (with guarantee $\alpha = 0.54$) for the two dimensional periodic potential in (7.1) and parameters (L, G) = (0.5, 1.5) with a discrete steady state gradient flow. (a) shows the support of $\rho^*(\mathbf{x})$. The support contains 0.9894 of the mass of $\rho^*(\mathbf{x})$. (b) shows the steady state solution of (1.6) with N = 1000 particles.

function $F_R(\mathbf{x})$. Developing alternative recovery methods with improved stability properties may therefore be important in the future.

8. Discussion and conclusions. In this paper we provide a new approach for systematically computing approximate minimizers to an energy that models pairwise interactions. This is done by relaxing the nonconvex optimization problem into a convex one to obtain a new sufficient condition for global minimizers. A recovery procedure is then introduced as a way to find candidate minimizers that satisfy the new sufficient condition (see Remark 3.5). The advantage of the approach is that the resulting convex relaxation may be described analytically, which then leads to numerical discretizations of the new condition that may be solved using well-known methods.

Analytically, the sufficient condition arises from a lower bound to the minimum energy of the nonconvex objective function. The new lower bound then provides a way to quantify how optimal a candidate minimizer is. The utility of the approach is demonstrated by the computation of a phase diagram for the periodic Morse potential, and also with the computation of minimizers for numerous interaction potentials in one and two dimensions. For example, a lattice of Dirac masses is shown to be the global minimum, for specific parameter values, in the periodic Morse potential. Verifying that a lattice is a global minimizer to a nonlocal energy is a difficult problem in mathematical physics, with great practical interest (see Remark 3.6). Hence, new approaches that can show when a lattice minimizes a nonlocal energy are of theoretical interest.

Last, a fundamental problem in the minimization of pairwise energies over probabilities is to identify sets S_* where the functional $\mathcal{E}(\rho)$ is convex, whenever the support of $\rho(\mathbf{x})$ is contained in S_* . To this end, our approach provides one way to identify such sets by exploiting a dual optimization problem. Specifically, the dual formulation results in an optimal decomposition of the energy functional $\mathcal{E}(\rho)$ into the sum of a convex and nonconvex functional. The resulting convex/nonconvex splitting can then be used to analytically identify supports in which $\mathcal{E}(\rho)$ is convex. From a physical perspective, this dual decomposition provides new insight into the natural length scales that many particle systems may self-assemble into and may eventually help in designing and controlling pattern formation in many particle systems.

Appendix A. Cases where the lower bound (R) is sharp. There are several straightforward cases where the lower bound (R) is sharp, and the recovery $\rho^*(\mathbf{x})$ is guaranteed to be the exact global minimum—even when $\mathcal{E}(\rho)$ is nonconvex. In this section we outline the known cases where (R) is sharp. We also characterize the corresponding dual decomposition obtained from (D) in the known exact cases.

Proposition A.1. For a $W(\mathbf{x})$ satisfying properties (W1)-(W4), $\rho_0(\mathbf{x}) = \delta(\mathbf{x})$ is a global minimizer to (P) if and only if $W(\mathbf{0}) \leq W(\mathbf{x})$ for all $\mathbf{x} \in \Omega$.

Proof. If $W(\mathbf{0}) \leq W(\mathbf{x})$ for all $\mathbf{x} \in \Omega$, set $\rho_0(\mathbf{x}) = \delta(\mathbf{x})$. Then for any probability distribution $\rho(\mathbf{x})$,

$$\mathcal{E}(\rho) = \frac{1}{2} \int_{\Omega} \int_{\Omega} W(\mathbf{x} - \mathbf{y}) \rho(\mathbf{x}) \rho(\mathbf{y}) \, d\mathbf{x} \, d\mathbf{y}$$
$$\geq \frac{1}{2} W(\mathbf{0}) \int_{\Omega} \int_{\Omega} \rho(\mathbf{x}) \rho(\mathbf{y}) \, d\mathbf{x} \, d\mathbf{y} = \mathcal{E}(\rho_0).$$

Hence $\rho_0(\mathbf{x})$ solves (P). To show the converse, take $\rho_0(\mathbf{x}) = \delta(\mathbf{x})$ as a global minimizer to (P) and assume by contradiction there exists an $\mathbf{s} \neq 0$ such that $W(\mathbf{s}) < W(\mathbf{0})$. Testing the energy with a candidate $\rho^*(\mathbf{x}) = \frac{1}{2}(\delta(\mathbf{x}) + \delta(\mathbf{x} - \mathbf{s}))$ yields

(A.1)
$$\mathcal{E}(\rho^*) = \frac{1}{4} (W(\mathbf{0}) + W(\mathbf{s}))$$

(A.2)
$$<\frac{1}{2}W(\mathbf{0}) = \mathcal{E}(\rho_0).$$

Hence, $\rho_0(\mathbf{x})$ cannot be a global minimizer and therefore $W(\mathbf{0}) \leq W(\mathbf{s})$ for all $\mathbf{s} \in \Omega$.

Remark A.2. What is interesting about Proposition A.1 is that the condition on $W(\mathbf{x})$ does not at all imply that $\mathcal{E}(\rho)$ is a convex functional. As an example, take $W(x) = -\cos(x)$ $\cos(2x) + 0.1 \cos(3x)$. Here W(0) is the minimum value of W(x) yet $\mathcal{E}(\rho)$ is nonconvex.

The following simple proposition is known in the literature, however, we repeat it here for completion.

Proposition A.3. Suppose W(x) satisfies properties (W1)-(W4) and, in addition, satisfies property (5.3), i.e.,

(A.3)
$$\sum_{\mathbf{k} \in \mathbb{Z}^d} \hat{W}(\mathbf{k}) < \infty, \quad \text{where} \quad \hat{W}(\mathbf{k}) := \langle W, \cos(2\pi \mathbf{k} \cdot \mathbf{x}) \rangle$$
(A.4)
$$and \quad W(\mathbf{x}) = \sum_{\mathbf{k} \in \mathbb{Z}^d} \hat{W}(\mathbf{k}) \cos(2\pi \mathbf{k} \cdot \mathbf{x}).$$

(A.4)
$$and \quad W(\mathbf{x}) = \sum_{\mathbf{k} \in \mathbb{Z}^d} \hat{W}(\mathbf{k}) \cos(2\pi \mathbf{k} \cdot \mathbf{x})$$

Then the function $\rho_0(\mathbf{x}) = 1$ is a global minimizer to (P) if and only if $\hat{W}(\mathbf{k}) \geq 0$ for all $\mathbf{k} \in \mathbb{Z}^d$.

Proof. If $\hat{W}(\mathbf{k}^*) < 0$ for some $\mathbf{k}^* \neq \mathbf{0}$, then $\rho^*(\mathbf{x}) = 1 + \cos(2\pi \mathbf{x} \cdot \mathbf{k}^*)$ has energy

$$\mathcal{E}(\rho^*) = \frac{1}{4} \langle W, \cos(2\pi \mathbf{k}^* \cdot \mathbf{x}) \rangle < 0 = \mathcal{E}(1).$$

Therefore the constant state is not the global minimum. To show the converse, substitute the cosine series expansion for $W(\mathbf{x})$ into $\mathcal{E}(\rho)$:

$$\mathcal{E}(\rho) = \frac{1}{2} \sum_{\mathbf{k} \in \mathbb{Z}^d} \hat{W}(\mathbf{k}) \Big(\langle \rho, \cos(2\pi \mathbf{k} \cdot \mathbf{x}) \rangle^2 + \langle \rho, \sin(2\pi \mathbf{k} \cdot \mathbf{x}) \rangle^2 \Big) \ge 0.$$

This series is justified by the regularity assumption in (A.3). Since $\hat{W}(\mathbf{k}) \geq 0$, the series expansion for $\mathcal{E}(\rho)$ over **k** is always nonnegative. Hence $\mathcal{E}(\rho) \geq 0 = \mathcal{E}(1)$.

Proposition A.4. Assume that $W(\mathbf{x})$ satisfies (W1)-(W4) and property (A.3). Then, the lower bound (R) is sharp when $\rho^*(\mathbf{x}) = 1$ or $\rho^*(\mathbf{x}) = \delta(\mathbf{x})$ is a global minimum to (P).

Proof. When $\rho^*(\mathbf{x}) = 1$, $W(\mathbf{x})$ has nonnegative cosine modes. The lower bound functional in (R) may then be expanded in a cosine series (again which is justified by (A.3)):

$$\langle F, W \rangle = \sum_{\mathbf{k} \in \mathbb{Z}^d} \hat{F}(\mathbf{k}) \hat{W}(\mathbf{k}) \ge 0 = \langle 1, W \rangle = \mathcal{E}_0.$$

Hence $F(\mathbf{x}) = 1$ is the minimizer to (R) over continuous functions, and $F_R(\mathbf{x}) = 1$ solves (R). Alternatively, if $\rho^*(\mathbf{x}) = \delta(\mathbf{x})$ is a global minimizer to (P), $W(\mathbf{0}) \leq W(\mathbf{x})$ for all $\mathbf{x} \in \Omega$. Hence, for any probability distribution $F(\mathbf{x})$.

$$\mathcal{E}_0 = \frac{1}{2}W(\mathbf{0}) = \frac{1}{2}\langle \delta(\mathbf{x}), W(\mathbf{x}) \rangle \le \langle F, W \rangle.$$

Therefore $F_R(\mathbf{x}) = \delta(\mathbf{x})$ solves (R) and is sharp.

In both cases, when $F_R(\mathbf{x}) = 1$ and $F_R(\mathbf{x}) = \delta(\mathbf{x})$, the solution $F_R(\mathbf{x})$ satisfies $F_R \circ F_R = 0$ F_R . Hence, taking $\rho^*(\mathbf{x}) = F_R(\mathbf{x})$, yields an exact recovery: $F_R(\mathbf{x}) = \rho^* \circ \rho^*$.

Remark A.5. The cases discussed in Proposition A.4 result in simple optimal dual decompositions:

• When $F_R(\mathbf{x}) = 1$ solves (R), the optimal dual decomposition is

$$W_R^+(\mathbf{x}) = 0, \quad K_R(\mathbf{x}) = W(\mathbf{x}), \quad \mathcal{E}_R = 0.$$

• When $F_R(\mathbf{x}) = \delta(\mathbf{x})$ solves (R) the optimal dual decomposition is

$$W_R^+(\mathbf{x}) = W(\mathbf{x}) - W(\mathbf{0}), \quad K_R(\mathbf{x}) = 0, \quad \mathcal{E}_R = \frac{1}{2}W(\mathbf{0}).$$

Appendix B. Numerical solution of (R). In this section we present numerical details regarding the solution of (R) and dual decomposition (D). We discuss explicit details in dimension d=1 and note that the extension to higher dimensions follows in a straightforward manner. To solve the relaxed problem, we use the MATLAB built-in optimization routines, which require the construction of matrices representing the linear constraints in (R).

Here we adopt the convention that vectors and matrices start with an index of 0 (as opposed to MATLAB) so that row indices coincide with Fourier mode numbers. For the general problem (R) we discretize space with an even number, n > 0, of points on an equispaced grid:

$$h = \frac{1}{n}$$
 $x_j = jh$ for $0 \le j \le n - 1$.

The functions W(x) and F(x) are then taken as n dimensional vectors $\mathbf{w}, \mathbf{f} \in \mathbb{R}^n$ so that

$$\mathbf{w}_j \approx W(x_j), \quad \mathbf{f}_j \approx F(x_j).$$

There are two choices for imposing the mirror (or odd) symmetry of \mathbf{f} . One can do it directly and set $\mathbf{f}_j = \mathbf{f}_{n-j}$, which will allow for a reduction in the number of variables to n/2; or one can build and enforce, a sine constraint matrix. For efficiency reasons, we adopt the direct approach; however we also describe how to construct the sine constraint matrix.

To build the matrices representing the sine and cosine constraints in (R), one may use the rows in the discrete Fourier transform matrix obtained via the fast Fourier transform. Meanwhile, for the nonnegativity constraint in (R), one may either use the MATLAB built-in nonnegativity constraint option, or directly enforce nonnegativity by passing the MATLAB routine a constraint matrix. Regardless of the option one uses, the three $n \times n$ constraint matrices can be constructed as follows:

Nonnegative constraint matrix: $\mathbf{P}_{lj} = -\delta_{lj}, \qquad 0 \leq l, j \leq n-1,$ Cosine mode matrix: $\mathbf{C}_{l,:} = -\text{real}\left(\text{fft}\left(\mathbf{e}_{l}\right)\right), \quad 0 \leq l \leq n-1,$ Sine mode matrix: $\mathbf{S}_{l} = \text{imag}\left(\text{fft}\left(\mathbf{e}_{l}\right)\right), \quad 0 \leq l \leq n-1.$

Here $\mathbf{C}_{l,:}$ and $\mathbf{S}_{l,:}$ are the entire *l*th matrix row, δ_{lj} is the Kronecker delta, and \mathbf{e}_l is the *l*th row of the $n \times n$ identity matrix:

$$\delta_{lj} = \begin{cases} 1 & \text{if } l = j, \\ 0 & \text{if } l \neq j, \end{cases} \quad \mathbf{e}_l = [0, 0, \dots, 0, 1, 0, \dots, 0].$$

By construction, the matrices have components $\mathbf{C}_{kj} = -\cos(2\pi kjh)$, $\mathbf{S}_{kj} = \sin(2\pi kjh)$ so that cosine and sine integrals are approximated via

(B.1)
$$-\langle \cos(2\pi kx), F(x) \rangle \approx h \sum_{j=0}^{n-1} \mathbf{C}_{kj} \mathbf{f}_j, \qquad \langle \sin(2\pi kx), F(x) \rangle \approx h \sum_{j=0}^{n-1} \mathbf{S}_{kj} \mathbf{f}_j.$$

To write the mass constraint in (R) explicitly, we also introduce the unit vector

$$\mathbf{1} = \begin{bmatrix} 1, 1, 1, \dots, 1 \end{bmatrix}^T \in \mathbb{R}^n.$$

Finally, note that by symmetry, the bottom half of the rows in matrices **C** and **S** are redundant. It is therefore sufficient to enforce constraints for only the rows of l with $1 \le l \le \lfloor \frac{n}{2} \rfloor$, where

$$\left\lfloor \frac{n}{2} \right\rfloor = \left\{ \begin{array}{ll} \frac{n}{2} & \text{if } n \text{ is even,} \\ \frac{n-1}{2} & \text{if } n \text{ is odd.} \end{array} \right.$$

The problem (R) then takes the discrete standard form

$$(R_h) \qquad \text{Minimize} \qquad \frac{1}{2} \mathbf{w}^T \mathbf{f}$$

$$\text{subject to} \quad \mathbf{P} \mathbf{f} \leq 0,$$

$$\mathbf{C}_{k,:} \mathbf{f} \leq 0, \qquad 1 \leq k \leq \left\lfloor \frac{n}{2} \right\rfloor,$$

$$\mathbf{S}_{k,:} \mathbf{f} = 0, \qquad 1 \leq k \leq \left\lfloor \frac{n}{2} \right\rfloor,$$

$$h \mathbf{1}^T \mathbf{f} = 1.$$

Problem (R_h) is then solved using a standard linear programming package with an interiorpoint algorithm. We use the MATLAB linprog routine, with a tolerance set to 10^{-8} . In pseudocode, the command takes the form

$$[\mathbf{f}_R, \mathcal{E}_R, \mathbf{W}^+, \mathbf{K}] = \text{linprog}(\mathbf{w}, constraint \ matrices \mathbf{P}, \mathbf{C}, \mathbf{S}, \mathbf{1}).$$

The output then consists of the optimal solution vector \mathbf{f}_R , the optimal solution value \mathcal{E}_R , as well as the dual decomposition vectors \mathbf{W}^+ and \mathbf{K} . In other words, the dual decomposition comes for free.

We identify two qualitatively different solutions \mathbf{f}_R to problem (R_h) .

Case 1: The solution \mathbf{f}_R converges as $h \to 0$ to a $C^0(\Omega)$ function with no Dirac mass singularities. In this case, the procedure from section 4 is used to recover a discrete $\rho^*(\mathbf{x})$ from \mathbf{f}_R . The vector $\rho^*(\mathbf{x})$ is discretized using n grid points on the same lattice as \mathbf{f}_R . The integrals in the continuous Schulz-Snyder algorithm are also computed using vectorized dot products (the standard midpoint rule is spectrally accurate for smooth solutions on periodic domains and lower order for nonsmooth solutions $F_R(\mathbf{x})$). The discrete $\rho^*(\mathbf{x})$ is computed to within steady state tolerances tol₁, tol₂ so that the discrete quantities satisfy

(B.2)
$$\mathcal{F}(\rho_n) - \mathcal{F}(\rho_{n+1}) < \text{tol}_1, \qquad \|\rho_{n+1} - \rho_n\|_{L^1(\Omega_h)} < \text{tol}_2,$$

(B.3) where
$$||f||_{L^1(\Omega_h)} := h \sum_{j=0}^{n-1} |f_j|.$$

Case 2: The solution $\mathbf{f} \to F_R(x)$ converges in distribution to a set of delta distributions as $h \to 0$. Namely, for any smooth function u(x) and corresponding discrete vector \mathbf{u} , the value $h(\mathbf{u}^T\mathbf{f}) \to \langle u(x), F_R(x) \rangle$ converges as $h \to 0$.

Remark B.1. In case 2, one may obtain delta masses in \mathbf{f}_R with a support of one mesh point each by modifying the grid size h to naturally accommodate the spacings between the delta masses. To do this, (i) obtain a solution \mathbf{f}_R (that may have delta masses smeared over a few grid points) to (R_h) with a suitably fine mesh h; (ii) estimate the distance between the Dirac masses in \mathbf{f}_R ; (iii) take a new grid spacing h', such that the distance between Delta masses is an integer multiple of h'; (iv) resolve the discrete problem $(R_{h'})$ using the new grid h' to obtain improved convergence. Improvements in the linear programming time were also observed when choosing a grid spacing h' that is commensurate with the spacings of the Dirac deltas.

Remark B.2. In two dimensions, we found that the solution \mathbf{f}_R to the linear program (R_h) can become sensitive to the exact number n, the prescribed tolerance, and the allowable number of interior-point iterations.

Remark B.3. We systematically ran hundreds of recovery tests and found that the Schulz–Snyder algorithm often converged to the same value $\mathcal{F}(\rho_{\infty})$ within numerical error. We did, however, observe that when $F_R(\mathbf{x})$ was a discrete probability measure in two dimensions, there were multiple $\rho^*(\mathbf{x})$ that minimized $\mathcal{F}(\rho)$. The different $\rho^*(\mathbf{x})$ had almost the same recovery guarantees α to within ± 0.02 .

Appendix C. Periodic effects for the solution to (R). The purpose of this section is to examine a simple subclass of minimizers $F_R(x)$ to (R) in one dimension. We show that provided W(x) satisfies a few regularity properties, minimizers within this subclass always have spacings that are commensurate with a discrete lattice. This will turn out to be a direct result of the periodic domain Ω .

In this section, we consider the restricted set of probabilities

(C.1)
$$F(x) = \alpha \delta(x) + \beta \delta(x-s) + \beta \delta(x+s),$$
$$\alpha + 2\beta = 1, \qquad 0 \le s \le \frac{1}{2}.$$

The subclass (C.1) is then completely characterized by two parameters (s, β) . The lower bound problem (R), restricted to the probabilities (C.1) with three delta masses, is

$$(R_3) \quad \text{minimize} \quad \frac{1}{2} \langle W(x), F(x) \rangle = \frac{1}{2} W(0) + \beta (W(s) - W(0)).$$

We now outline why unique minimizers of the form (C.1) to (R_3) , characterized by values (s^*, β^*) , often have support commensurate with a lattice; that is, $s^* \in \mathbb{Q}$ is a rational number.

First optimize the energy (R_3) at a fixed s, over the weight β , thereby yielding a function only of s:

$$E(s) := \frac{1}{2}W(0) + \inf_{\beta} \left[\beta \left(W(s) - W(0) \right) \right].$$

If $W(0) \le W(s)$, then $E(s) = \frac{1}{2}W(0)$, which occurs when $\beta = 0$. If W(0) > W(s), then E(s) takes the following form,

$$E(s) = \frac{1}{2}W(0) + \theta(s)(W(s) - W(0)),$$
(C.2)
$$\theta(s) := \sup \beta \quad \text{subject to} \quad (1 - 2\beta)\delta(x) + \beta\delta(x - s) + \beta\delta(x + s) \in \mathcal{C}.$$

The function $\theta(s)$ can be computed by examining the convex cone constraint $F(x) \in \mathcal{C}$:

$$\langle F, \cos(2\pi kx) \rangle = 1 - 2\beta + 2\beta \cos(2\pi ks) \ge 0$$
 for all $k \in \mathbb{Z} \setminus 0$.

Hence,

$$0 \le \beta \le \frac{1}{2(1 - \cos(2\pi ks))}$$
 for all $k \in \mathbb{Z} \setminus 0$.

It follows that,

$$\theta(s) = \inf_{k \in \mathbb{Z} \setminus 0} \frac{1}{2(1 - \cos(2\pi ks))}$$

When the value of s is irrational (denote by $\overline{\mathbb{Q}}$), $\cos(2\pi ks)$ can be made arbitrarily close to -1:

$$\theta(s) = \frac{1}{4} \text{ for } s \in \overline{\mathbb{Q}}, \qquad \theta(s) = \min_{0 \le k \le p} \frac{1}{2(1 - \cos(2\pi k s))} \text{ for } s = \frac{q}{p} \in \mathbb{Q}.$$

An immediate consequence is that $\theta(q/p) \geq \theta(s)$ for all $q/p \in \mathbb{Q}$ (rational) and $s \in \overline{\mathbb{Q}}$ (irrational). The function $\theta(s)$ also has interesting continuity properties.

Proposition C.1. The function $\theta(s)$ for $0 < s < \frac{1}{2}$, is continuous at all $s \in \overline{\mathbb{Q}} \cup \mathbb{Q}_e$, and discontinuous at all $s \in \mathbb{Q}_o$, where $\mathbb{Q} = \mathbb{Q}_e \cup \mathbb{Q}_o$:

$$\mathbb{Q}_e = \{q/p \in \mathbb{Q} : gcd(q, p) = 1, p \text{ even}\}, \qquad \mathbb{Q}_o = \{q/p \in \mathbb{Q} : gcd(q, p) = 1, p \text{ odd}\}.$$

Proof. For simplicity in the proof first introduce

$$\tilde{\theta}(s) := -1 \text{ for } s \in \overline{\mathbb{Q}}, \quad \tilde{\theta}(s) = \min_{0 \le k \le p} \cos(2\pi k s) \text{ for } s := \frac{q}{p} \in \mathbb{Q}.$$

Since $\theta(s)$ is a composition of a continuous function with $\tilde{\theta}(s)$, it is sufficient to prove Proposition C.1 for the modified function $\tilde{\theta}(s)$ instead of $\theta(s)$.

First we remark on the value of $\tilde{\theta}(q/p)$ for integers q, p with $\gcd(q, p) = 1$: there exists an integer $k^* > 0$ such that

$$k^*q \equiv \frac{p}{2} \pmod{p}$$
 if p is even,
 $k^*q \equiv \frac{p+1}{2} \pmod{p}$ if p is odd.

Hence the optimal value of $\tilde{\theta}(s)$ is given by

$$\tilde{\theta}(q/p) = \cos\left(\frac{2\pi k^* q}{p}\right) = \cos(\pi) = -1 \qquad \text{if } p \text{ is even,}$$

$$\tilde{\theta}(q/p) = \cos\left(\frac{2\pi k^* q}{p}\right) = \cos\left(\pi + \frac{\pi}{p}\right) = -\cos\left(\frac{\pi}{p}\right) \quad \text{if } p \text{ is odd.}$$

If $s_0 \in \mathbb{Q}_o$, then any sequence $s_i \to s_0$ with $s_i \in \overline{\mathbb{Q}}$ has

$$\tilde{\theta}(s_0) - \tilde{\theta}(s_j) = \tilde{\theta}(s_0) + 1 > \delta > 0$$
 for some δ .

Hence $\tilde{\theta}(s)$ is discontinuous at \mathbb{Q}_o .

For continuity at a point $s_0 \in \overline{\mathbb{Q}} \cup \mathbb{Q}_e$, let $\epsilon > 0$. Clearly for any $s \in \overline{\mathbb{Q}} \cup \mathbb{Q}_e$,

$$|\tilde{\theta}(s) - \tilde{\theta}(s_0)| = 0 < \epsilon.$$

To examine the behavior of $s \in \mathbb{Q}_o$, fix $t = \lceil \epsilon^{-1} \rceil$ as the smallest integer larger than ϵ^{-1} . Note that there are only a finite number of rational numbers q/p with $p \le t$ (and $\gcd(q,p) = 1$) in the interval $s_0 - 1 < q/p < s_0 + 1$. Hence, for any $\epsilon > 0$, one may take $\delta = \delta(\epsilon)$ small enough so that the rational value q/p satisfying $|s_0 - q/p| < \delta$ must have p > t. Consequently for any rational $q/p \in \mathbb{Q}_o$,

$$\Longrightarrow \left| \tilde{\theta}(q/p) - \tilde{\theta}(s_0) \right| = \left| \cos \left(\pi + \frac{\pi}{p} \right) - \cos(\pi) \right| \le \frac{\pi}{p} \le \frac{\pi}{t} \le \pi \epsilon.$$

In the last line we used a Lipschitz constant of 1 for cosine. This concludes the proof.

Proposition C.1 now leads to the following result: if W(s) is smooth enough, s^* must be rational.

Proposition C.2. Suppose W(s) satisfies (W1)–(W4) and has a bounded second derivative on (0,1). Assume also that $W(0) > \min_{0 < x < 1} W(x)$ is not the strict minimum value of W(x). Fix $0 < s^* < \frac{1}{2}$ with $s^* \in \overline{\mathbb{Q}} \cup \mathbb{Q}_e$. Then s^* does not minimize E(s).

Proof. We assume that $s^* \in \overline{\mathbb{Q}} \cup \mathbb{Q}_e$ minimizes E(s), and then arrive at a contradiction. First observe that if $s^* \in \overline{\mathbb{Q}} \cup \mathbb{Q}_e$ and minimizes E(s), then s^* must also minimize W(s). This is because $E(s^*) = \frac{1}{4}(W(s^*) + W(0))$ whenever $s^* \in \overline{\mathbb{Q}} \cup \mathbb{Q}_e$. Hence, by continuity of W(s), s^* must minimize W(s) and therefore $W'(s^*) = 0$. Using Taylor's remainder theorem, there exists a constant C such that for any s in the neighborhood of s^* ,

$$|W(s) - W(s^*)| \le C|s - s^*|^2$$
.

We now argue that one can find a rational point close to s^* that has a lower value of E(s) than $E(s^*)$. Using basic properties of cosine, as well as the result from Proposition C.1, one has that for any rational point $q/p \in \mathbb{Q}_o$ in the neighborhood of s^* , there exists a $c_1 > 0$ such that

$$\left|\tilde{\theta}(q/p) - \tilde{\theta}(s^*)\right| = \left|\cos\left(\frac{\pi}{p} + \pi\right) - \cos(\pi)\right| \ge \frac{c_1}{p^2}.$$

Now consider a sequence of approximating rational points $s_j = q_j/p_j \to s^*$ for j > 0 with $s_j \in \mathbb{Q}$ that by a well-known theorem from continued fractions [31] satisfy

$$\left| \frac{q_j}{p_j} - s^* \right| \le \frac{c_2}{p_j^2}.$$

An important remark, is that the sequence of p_j generated via continued fractions have p_j odd infinitely often. Therefore, without loss of generality we may restrict the sequence s_j to a subsequence on \mathbb{Q}_o that has p_j odd.¹⁰

Hence, combining the previous two inequalities, on this sequence $s_j \in \mathbb{Q}_o$

$$|\theta(s_j) - \theta(s^*)| \ge c_3 |s_j - s^*|.$$

By direct calculation, for j sufficiently large,

(C.3)
$$E(s_j) - E(s^*) = \theta(s_j) \Big(W(s_j) - W(s^*) \Big) + \Big(\theta(s_j) - \theta(s^*) \Big) \Big(W(s^*) - W(0) \Big)$$

(C.4)
$$\leq A_1 |s_j - s^*|^2 - A_2 |s_j - s^*|,$$

where $A_1 > 0$ is an upper bound on $\theta(s_j)$ and the Taylor constant, $A_2 = c_3(W(0) - W(s^*)) > 0$. Finally, for sufficiently large j one has $A_2|s_j - s^*| > A_1|s_j - s^*|^2$ implying

$$E(s_j) < E(s^*).$$

Thus, s^* cannot minimize E(s).

The purpose of Proposition C.2 is to observe that if W(s) is smooth enough on (0,1), then minimizations of the form (C.1) must have rational spacings.

Acknowledgments. The author (DS) would like to thank Ihsan Topaloglu for many insightful comments regarding pairwise interaction problems. The authors have also greatly benefited from conversations with Rustum Choksi, Robert Kohn, Cyrill Muratov, and Jennifer Park. The authors would also like to thank the anonymous reviewers for many comments that helped to improve the presentation of the paper.

REFERENCES

- [1] A. Ahmed, B. Recht, and J. Romberg, Blind deconvolution using convex programming, IEEE Trans. Inform. Theory, 60 (2013), pp. 1711–1732.
- [2] B. AMES AND S. VAVASIS, Convex optimization for the planted k-disjoint-clique problem, Math. Program., 143 (2014), pp. 299–337.
- [3] D. Balagué, J. Carrillo, T. Laurent, and G. Raoul, Dimensionality of local minimizers of the interaction energy, Arch. Ration. Mech. Anal., 209 (2013), pp. 1055–1088.

¹⁰An infinite continued fraction can be represented as a unique sequence of positive integers $(a_0, a_1, a_2, ...)$. The rational $s_j = q_j/p_j$ approximations satisfy the recursion relations $q_0 = a_0$, $p_0 = 1$, $q_1 = a_1a_0 + 1$, $p_1 = a_1$, and $q_j = a_jq_{j-1} + q_{j-2}$, $p_j = a_jp_{j-1} + p_{j-2}$, for $j \ge 2$. Therefore using an induction argument, one can show that if (p_{j-1}, p_j) has at least one odd term, then (p_{j+1}, p_{j+2}) also has one odd term. Since $(p_0, p_1) = (1, a_1)$, the result follows.

- [4] D. BALAGUÉ, J. CARRILLO, AND Y. YAO, Confinement for repulsive-attractive kernels, Discrete Contin. Dyn. Syst. Ser. B, 19 (2014), pp. 1227–1248.
- [5] A. J. Bernoff and C. M. Topaz, Nonlocal aggregation models: A primer of swarm equilibria, SIAM Rev., 55 (2013), pp. 709–747.
- [6] S. BOYD AND L. VANDENBERGHE, Convex Optimization, Cambridge University Press, Cambridge, 2004.
- [7] R. BURACHIK AND V. JEYAKUMAR, A simple closure condition for the normal cone intersection formula, Proc. Amer. Math. Soc., 133 (2005), pp. 1741–1748.
- [8] J. A. CAÑIZO, J. A. CARRILLO, AND F. S. PATACCHINI, Existence of compactly supported global minimisers for the interaction energy, Arch. Ration. Mech. Anal., 217 (2015), pp. 1197–1217.
- [9] E. CANDÈS AND X. LI, Solving quadratic equations via phaselift when there are about as many equations as unknowns, Found. Comput. Math., 14 (2014), pp. 1017–1026.
- [10] E. CANDÈS, X. LI, AND M. SOLTANOLKOTABI, Phase retrieval via Wirtinger flow: Theory and algorithms, IEEE Trans. Inform. Theory, 61 (2015), pp. 1985–2007.
- [11] E. CANDÈS AND T. TAO, The power of convex relaxation: Near-optimal matrix completion, IEEE Trans. Inform. Theory, 56 (2010), pp. 2053–2080.
- [12] J. CARRILLO, A. FIGALLI, AND F. PATACCHINI, Geometry of minimizers for the interaction energy with mildly repulsive potentials, Ann. Inst. H. Poincaré Anal. Non Linéaire, 34 (2016), pp. 1299–1308, https://doi.org/10.1016/j.anihpc.2016.10.004.
- [13] J. A. CARRILLO, M. CHIPOT, AND Y. HUANG, On global minimizers of repulsive-attractive power-law interaction energies, R. Soc. Phil. Trans. Lond. A Math. Phys. Eng. Sci., 372 (2014), 0399, https://doi.org/10.1098/rsta.2013.0399.
- [14] J. A. CARRILLO, D. SLEPČEV, AND L. WU, Nonlocal-interaction equations on uniformly prox-regular sets, Discrete Contin. Dyn. Syst., 36 (2016), pp. 1209–1247.
- [15] R. CHOKSI, R. FETECAU, AND I. TOPALOGLU, On minimizers of interaction functionals with competing attractive and repulsive potentials, Ann. Inst. H. Poincaré Anal. Non Linéaire, 32 (2015), pp. 1283– 1305.
- [16] H. Cohn, A. Kumar, and A. Schurmann, Ground states and formal duality relations in the Gaussian core model, Phys. Rev. E (3), 80 (2009), 061116.
- [17] M. A. COTTER, Hard spherocylinders in an anisotropic mean field: A simple model for a nematic liquid crystal, J. Chem. Phys., 66 (1977), pp. 1098–1106.
- [18] K. CRAIG AND I. TOPALOGLU, Convergence of regularized nonlocal interaction energies, SIAM J. Math. Anal., 48 (2016), pp. 34–60.
- [19] L. DEMANET AND P. HAND, Scaling law for recovering the sparsest element in a subspace, Inf. Inference, 3 (2014), pp. 295–309.
- [20] W. E AND D. LI, On the crystallization of 2d hexagonal lattices, Comm. Math. Phys., 286 (2009), pp. 1099–1140.
- [21] M. EMELIANENKO, Z.-K. LIU, AND Q. DU, A new algorithm for the automation of phase diagram calculation, Comput. Mater. Sci., 35 (2006), pp. 61–74.
- [22] B. FARMER, S. ESEDOĞLU, AND P. SMEREKA, Crystallization for a Brenner-like potential, Comm. Math. Phys., 349 (2016), pp. 1029–1061, https://doi.org/10.1007/s00220-016-2732-6.
- [23] C. Floudas, Deterministic Global Optimization, Theory, Methods and Applications, Kluwer Academic, Dordrecht, the Netherlands, 2000.
- [24] G. B. FOLLAND, Real Analysis: Modern Techniques and Their Applications, 2nd ed., Wiley, New York, 1999.
- [25] M. GOEMANS AND D. WILLIAMSON, Improved approximation algorithms for maximum cut and satisfiability problems using semidefinite programming, J. ACM, 42 (1995), pp. 1115–1145.
- [26] J.-P. HARVEY, G. ERIKSSON, D. ORBAN, AND P. CHARTRAND, Global minimization of the Gibbs energy of multicomponent systems involving the presence of order/disorder phase transitions, Amer. J. Sci., 313 (2013), pp. 199–241.
- [27] R. C. HEITMANN AND C. RADIN, The ground state for sticky disks, J. Stat. Phys., 22 (1980), pp. 281–287.
- [28] J.-B. Hiriart-Urruty and A. Seeger, A variational approach to copositive matrices, SIAM Rev., 52 (2010), pp. 593–629.
- [29] M. HOLMES-CERFON, S. J. GORTLER, AND M. P. BRENNER, A geometrical approach to computing energy landscapes from short-ranged potentials, Proc. Natl. Acad. Sci. USA, 110 (2013), pp. E5–E14.

- [30] K. JAGANATHAN, S. OYMAK, AND B. HASSIBI, Recovery of sparse 1d signals from the magnitudes of their Fourier transform, 2012 IEEE International Symposium on Information Theory Proceedings (ISIT), IEEE, Piscataway, NJ, (2012), pp. 1473–1477.
- [31] W. Jones and W. J. Thron, Continued Fractions. Analytic Theory and Applications, Encyclopaedia of Math. Appl. 11, Addison-Wesley, Reading, MA, 1980.
- [32] R. LAI, J. LIU, AND S. OSHER, Density matrix minimization with ℓ₁ regularization, Comm. Math. Sci., 13 (2015), pp. 2097–2117.
- [33] A. J. LEVERENTZ, C. M. TOPAZ, AND A. J. BERNOFF, Asymptotic dynamics of attractive-repulsive swarms, SIAM J. Appl. Dyn. Syst., 8 (2009), pp. 880–908.
- [34] M. LOCATELLI AND F. SCHOEN, Efficient algorithms for large scale global optimization: Lennard-Jones clusters, Comput. Optim. Appl., 26 (2003), pp. 173–190.
- [35] M. LOCATELLI AND F. SCHOEN, Global Optimization: Theory, Algorithms and Applications, MOS-SIAM Ser. Optim., SIAM, Philadelphia, 2013.
- [36] J. Lu and F. Otto, An isoperimetric problem with Coulomb repulsion and attraction to a background nucleus, preprint, arXiv:1508.07172, 2015.
- [37] C. D. MARANAS AND C. A. FLOUDAS, Global minimum potential energy conformations of small molecules, J. Global. Optim., 4 (1994), pp. 135–170.
- [38] E. MARCOTTE, F. STILLINGERB, AND S. TORQUATO, Optimized monotonic convex pair potentials stabilize low-coordinated crystals, Soft Matter, 7 (2011), pp. 2332–2335.
- [39] P. MASSART, Concentration Inequalitites and Model Selection, Lecture Notes in Math. 1896, Springer, Berlin, 2007.
- [40] A. MOGILNER, L. EDELSTEIN-KESHET, L. BENT, AND A. SPIROS, Mutual interactions, potentials, and individual distance in a social aggregation, J. Math. Biol., 47 (2003), pp. 353–389.
- [41] S. MOTSCH AND E. TADMOR, Heterophilious dynamics enhances consensus, SIAM Rev., 56 (2014), pp. 577–621.
- [42] Y. Nesterov, H. Wolkowicz, and Y. Ye, Semidefinite programming relaxations of nonconvex quadratic optimization, in Handbook of Semidefinite Programming, Vol. 27, Springer, 2000, pp. 361–419.
- [43] M. NOURALISHAHI, C. Wu, and L. Vandenberghe, Model calibration for optical lithography via semidefinite programming, Optim. Eng., 9 (2008), pp. 19–35.
- [44] Onsager, The effects of shape on the interaction of colloidal particles, Ann. N.Y. Acad. Sci., 51 (1949), pp. 627–659.
- [45] C. Radin, The ground state for soft disks, J. Stat. Phys., 26 (1981), pp. 365-373.
- [46] M. RECHTSMAN, F. STILLINGER, AND S. TORQUATO, Optimized interactions for targeted self-assembly: Application to a honeycomb lattice, Phys. Rev. Lett., 95 (2005), 228301.
- [47] T. ROCKAFELLAR, Convex Analysis, Princeton Math. Ser. 28, Princeton University Press, Princeton, NJ, 1970.
- [48] W. Rudin, Real and Complex Analysis, 3rd ed., McGraw-Hill, Singapore, 1987.
- [49] A. S. Schneider, C. J. Horowitz, J. Hughto, and D. K. Berry, *Nuclear pasta formation*, Phys. Rev. C (3), 88 (2013), 065807.
- [50] T. SCHULZ AND D. SNYDER, Image recovery from correlations, J. Optical. Soc. Amer. A, 9 (1992), pp. 1266–1272.
- [51] T. Schulz and D. Voelz, Signal recovery from autocorrelation and cross-correlation data, J. Optical. Soc. Amer. A, 22 (2005), pp. 616–624.
- [52] D. Shirokoff, R. Choksi, and J.-C. Nave, Sufficient conditions for global minimality of metastable states in a class of non-convex functionals: A simple approach via quadratic lower bounds, J. Nonlinear Sci., 25 (2015), pp. 539–582.
- [53] R. Simione, D. Slepčev, and I. Topaloglu, Existence of ground states of nonlocal-interaction energies, J. Stat. Phys., 159 (2015), pp. 972–986.
- [54] A. SÜTŐ, Crystalline ground states for classical particles, Phys. Rev. Lett., 95 (2005), 265501.
- [55] A. SÜTŐ, From bcc to fcc: Interplay between oscillating long-range and repulsive short-range forces, Phys. Rev. B (3), 74 (2006), 104117.
- 56] A. Süтő, Ground state at high density, Comm. Math. Phys., 305 (2011), pp. 657-710.
- [57] F. THEIL, A proof of crystallization in two dimensions, Comm. Math. Phys., 262 (2006), pp. 209–236.
- [58] S. Torquato, Necessary conditions on realizable two-point correlation functions of random media, Ind. Eng. Chem. Res., 45 (2006), pp. 6923–6928.

- [59] J. VON BRECHT, D. UMINSKY, T. KOLOKOLNIKOV, AND A. BERTOZZI, *Predicting pattern formation in particle interactions*, Math. Models Methods Appl. Sci., 22 (2012), 1140002.
- [60] I. Waldspurger, A. d'Aspremont, and S. Mallat, *Phase recovery, maxcut and complex semidefinite programming*, Math. Program., 149 (2015), pp. 47–81.
- [61] X. R. Wang, J. M. Miller, J. Lizier, M. Prokopenko, and L. Rossi, *Quantifying and tracing information cascades in swarms*, PloS ONE, 7 (2012), e40084.